



This is a repository copy of *Effective T-matrix of a cylinder filled with a random two-dimensional particulate*.

White Rose Research Online URL for this paper:

<https://eprints.whiterose.ac.uk/214277/>

Version: Published Version

Article:

Napal, K.K. orcid.org/0000-0003-2901-5655, Piva, P.S. and Gower, A.L. (2024) Effective T-matrix of a cylinder filled with a random two-dimensional particulate. *Proceedings of the Royal Society A: Mathematical, Physical and Engineering Sciences*, 480 (2292). 20230660. ISSN 1364-5021

<https://doi.org/10.1098/rspa.2023.0660>

Reuse

This article is distributed under the terms of the Creative Commons Attribution (CC BY) licence. This licence allows you to distribute, remix, tweak, and build upon the work, even commercially, as long as you credit the authors for the original work. More information and the full terms of the licence here:

<https://creativecommons.org/licenses/>

Takedown

If you consider content in White Rose Research Online to be in breach of UK law, please notify us by emailing eprints@whiterose.ac.uk including the URL of the record and the reason for the withdrawal request.



eprints@whiterose.ac.uk
<https://eprints.whiterose.ac.uk/>



Research

**Cite this article:** Napal KK, Piva PS, Gower AL.2024 Effective T-matrix of a cylinder filled with a random two-dimensional particulate. *Proc. R. Soc. A* **480**: 20230660.<https://doi.org/10.1098/rspa.2023.0660>

Received: 7 September 2023

Accepted: 25 March 2024

Subject Areas:

mathematical physics

Keywords:

multiple scattering, random media, effective media, ensemble average wave motion, acoustics, statistical physics

Author for correspondence:

K. K. Napal

e-mail: kevish.napal@gmail.com

One contribution to a special feature “Mathematical theory and applications of multiple wave scattering” organised by guest editors Luke G. Bennetts, Michael H. Meylan, Malte A. Peter, Valerie J. Pinfield and Olga Umnova.

Effective T-matrix of a cylinder filled with a random two-dimensional particulate

K. K. Napal, P. S. Piva and A. L. Gower

Department of Mechanical Engineering, University of Sheffield, Sheffield, UK

KKN, 0000-0003-2901-5655

When a wave, such as sound or light, scatters within a densely packed particulate, it can be rescattered many times between the particles, which is called multiple scattering. Multiple scattering can be unavoidable when trying to use sound waves to measure a dense particulate, such as a composite with reinforcing fibres. Here, we solve from first principles multiple scattering of scalar waves, including acoustic, for any frequency from a set of two-dimensional particles confined in a circular area. This case has not been solved yet, and its solution is important to perform numerical validation, as particles within a cylinder require only a finite number of particles to perform direct numerical simulations. The method we use involves ensemble averaging over particle configurations, which leads us to deduce an effective T-matrix for the whole cylinder, which can be used to easily describe the scattering from any incident wave. In the specific case when the particles are monopole scatterers, the expression of this effective T-matrix simplifies and reduces to the T-matrix of a homogeneous cylinder with an effective wavenumber k_* . To validate our theoretical predictions, we develop an efficient Monte Carlo method and conclude that our theoretical predictions are highly accurate for a broad range of frequencies.

1. Introduction

(a) Ensemble averaging

Multiple scattering is unavoidable when using waves to characterize a particulate composite, or designing

metamaterials to control wave propagation. Furthermore, the number of particles in most applications makes direct numerical simulations impossible for current computing power, though there are some notable attempts [1,2]. Even if such simulations were possible, when it comes to experimental measurements, the positions of the particles are impossible to know for one particular sample. One way to avoid these problems is to use ensemble averaging. That is, to take an average over all possible particle positions. In light or acoustic experiments conducted for fluids and gases, this type of averaging occurs naturally when averaging over time as the particles are rapidly moving around. That is, taking an average of the scattered signal over time can be equivalent to an ensemble average.¹ Assuming that ensemble averaging is equivalent to averaging over time and space, which is often the case, is called the ergodicity assumption [3]. Refer to [4–6] for work that compares the ensemble-averaged field approach with the cases of one specific configuration of particles.

(b) What is known

The scenarios that are best understood are (i) waves in an infinite medium with no boundaries [7,8] and (ii) plane waves incident on a half-space or plate filled with particles [6,9,10]. Both scenarios have been considered to obtain effective wavenumbers [11–13]. Though we mention the methods that use Lippmann–Schwinger for acoustics, they involve an extra integral that is often omitted [14] and complicates the calculations. Our approach in this article is valid for any type of scatterer and scalar waves. Both scenarios of using plane waves and an infinite medium have several applications (typically when considering layered media such as planetary atmospheres, layers in the ocean or soils), but one significant drawback is that it has been very challenging to numerically validate the assumptions used for these methods. Both use statistical assumptions, such as the quasi-crystalline approximation (QCA) [15] that is not based on an asymptotic approximation. Validation is needed to establish the range of validity of these assumptions. However, direct numerical simulations of scattering from a configuration of particles for both planes and infinite media require a huge number of particles [16,17] or the introduction of periodic boundaries, which can introduce artefacts [18].

(c) The cylindrical setting

The methods developed to describe the average plane wave propagating in a disordered particulate plate or half-space can now be extended to other geometries [19]. The ideal scenario to compare theoretical predictions with direct numerical simulations is to have cylindrical particles inside a cylinder, as this reduces the problem to two dimensions and we need only a finite number of particles for the direct numerical simulations. See [figure 1](#) for an illustration. This is the simplest case to perform numerical validation of a very general theory [19]. Furthermore, we show in this work that the effective dispersion equation for the cylindrical geometry is the same as the plane-wave case. So numerically validating the cylindrical geometry will also serve as numerical validation of the dispersion equation for plane waves and all geometries. We also note that it appears that the cylindrical setting has never been solved from a first principles approach. The formulas we provide are also valid for any inter-particle pair correlation. For a radiative transfer model of this setting, see [20].

¹In ergodic systems, if enough time has passed, all physically possible states of the system will have occurred, and so that taking an average over time is equivalent to averaging over all possible configurations.

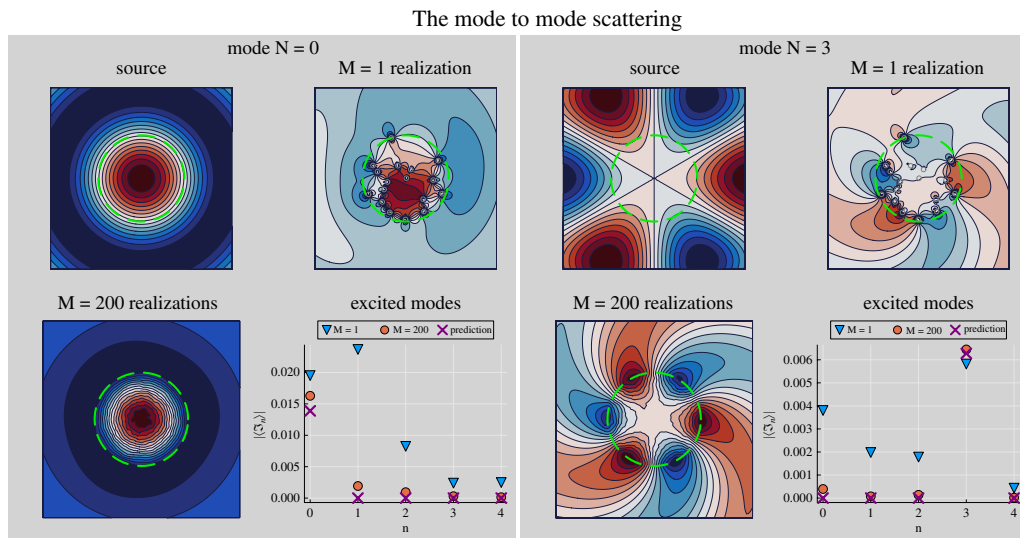


Figure 1. Consider a circular region filled with sound-hard particles, illuminated with a modal source of the form $u_{\text{inc}} = V_N(\mathbf{r})$ as defined in equation (2.3), with $N = 0$ (left panel) or $N = 3$ (right panel). Both panels compare the average scattered wave $\langle u_{\text{sc}} \rangle$ predicted by our effective wave method (EWM) with a brute force Monte Carlo (MC) approach. The MC approach simulates the scattered field from either 1, $M = 1$, or 200, $M = 200$, configurations of particles and then takes the average over these configurations. In general, the average scattered wave is given by equation (2.15). The left panel shows that when using an incident wave $u_{\text{inc}} = V_0(\mathbf{r})$, with radial symmetry, then the only scattered mode also has radial symmetry after averaging. The right panel shows how a source with a 60° rotation symmetry also leads to a scattered wave with the same symmetry.

(d) Industrial applications

Beyond numerical validation, there are industrial applications that need a method to calculate waves scattered from a cylinder with particles. Examples of cylinders filled with cylindrical particles include concrete beams reinforced with iron, cables filled with wires or fibre-reinforced composite [21]. Applications include designing cylinders with exotic effective properties or developing methods to measure the cylindrical particles [22,23]. In terms of measurement, it is likely that more information can be extracted from waves scattered from a cylinder filled with a particulate than just plane wave reflection from a plate filled with the same particulate.

(e) Effective properties

The most common approach to model the average scattering from, say, a spherical or cylindrical region with particles is to assume the region is homogeneous with some effective properties [24–30], and then use the standard boundary conditions such as continuity of displacement. This approach is valid for low frequency [28] but for higher frequencies is incorrect in three dimensions [19], and we demonstrate the same here for two dimensions in this work. To obtain an accurate model for broad-range frequencies, the boundary condition needs to be deduced from first principles, together with an eigensystem for the effective wavenumbers [19]. Although the process is more involved, the final expression for the average scattered wave from a cylindrical region is simple: the average scattered wave can be calculated from an effective T-matrix for any incident frequency, source and particle properties. We stress that without deducing the results from first principles, as we do here, it would not be possible to just guess the form of this effective T-matrix.

(f) Monopole scatterers

One somewhat surprising result we deduce is that if the particles scatter only monopole waves, that is, waves that have radial symmetry, then the material as a whole behaves as homogeneous, where the mass density is the same as the background, and the bulk density is given by a simple formula. We deduce this for particles in a cylinder and hypothesize that it is true for any material filled with monopole scatterers, even when including all orders of multiple scattering. Beyond just curiosity, there are many particles that behave approximately like a monopole scatterer, and therefore the simple formulas we deduced are appropriate. For example, in acoustics void-like, particles are approximately monopoles for a broad frequency range, see the Dirichlet case in [figure 2](#). In elasticity, particles become approximately monopole when the bulk modulus is much greater than the shear modulus [31]. Other cases include resonators such as a split ring resonator [32].

(g) Overview of the method

After ensemble averaging over particle configurations within a cylindrical region, the system inherits cylindrical symmetry. For example, if the source has radial symmetry, then the average scattered field will also have radial symmetry. This is also true for sources with more general rotational symmetry resulting in scattered fields of the same rotational symmetry (cf. [figure 1](#)). In this article, we take advantage of this mode-to-mode symmetry to analyse the general behaviour of the random particulate material independently from the incident field.

After denoting with V_n and U_n the regular and outgoing cylindrical waves of order n (cf. [equation \(2.3\)](#)), the cylindrical symmetry translates as follows: when the exciting source is V_n then the average scattered field is $T_n U_n$ where the complex number T_n only depends on the properties of the random particulate cylinder (radius and properties of the particles). Since the scattering problem is linear, the knowledge of the T_n allows us to describe the scattering from any incident field, after decomposing the latter into the modes V_n . Having simple expressions for T_n is crucial to help guide methods to characterize or design particulate materials. We do so by using the effective wave method (EWM) approach [19]. Finally, we validate our results with an adapted Monte Carlo (MC) method in which the rate of convergence is accelerated thanks to the cylindrical symmetry.

(h) Overview of this article

In §2, we first introduce the statistics of the random particulate material and the required notations for the ensemble averaging. We then define the T-matrix of the effective cylinder whose exact formula depends on the solutions of the averaged Foldy–Lax equations.

The latter are solved in §3 using the EWM, which consists of finding solutions that are isotropic waves with a complex wavenumber k_\star . The method leads to an eigenvalue problem called the dispersion equation, whose eigenvalue provides k_\star .

In §4, we use the expression of the solutions of the averaged Foldy–Lax equations to deduce a formula of the effective T-matrix. The latter is very simple when the particles are monopole scatterers:

$$T_n = -\frac{c_n}{\mathcal{D}_n} \quad \text{with} \quad \begin{cases} c_n &= k'_n(k\tilde{R})J_n(k_\star\tilde{R}) - k_\star J_n(k\tilde{R})J'_n(k_\star\tilde{R}) \\ \mathcal{D}_n &= kH'_n(k\tilde{R})J_n(k_\star\tilde{R}) - k_\star H_n(k\tilde{R})J'_n(k_\star\tilde{R})' \end{cases} \quad (1.1)$$

where \tilde{R} is the radius of the region enclosing the centres of the particles and k is the wave-number of the background medium. This result is remarkable because the above expression corresponds to the T-matrix of a homogeneous acoustic cylinder of radius \tilde{R} , sound speed

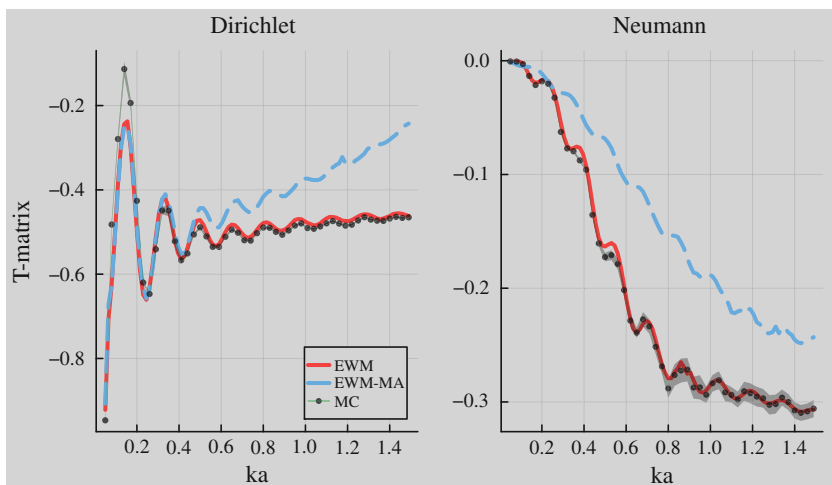


Figure 2. Comparison of various methods to calculate the component T_0 of the T-matrix of a cylinder filled with particles. The solid red line is our effective waves method (EWM) (equation (1.2)), the black points are from a brute force MC method and the dashed blue line is our method when only monopole scattering is accounted for (EWM-MA) (equation (1.1)). The left (right) graph shows the results for sound soft (hard) particles. In both cases, the general expression of the effective T-matrix matches the MC results. The EWM-MA method only matches well with the MC for sound soft scatterers for low frequencies. Both graphs were generated with a particulate volume fraction of $n = 0.05$ (portion area occupied by particles of radius $a = 1$ inside the cylinder of radius $R = 20$).

$c_\star = \omega/k_\star$ and density ρ , which is equal to the background medium. Particles that are approximately monopole scatterers appear in mainly two scenarios: either small sound soft particles or resonators [33]. For all these cases, the T-matrix being given by equation (1.1) shows us that the effective wavenumber k_\star suffices to describe the random material.

When the particles are not monopole scatterers, equation (1.1) is not exact. The exact formula is given by

$$T_n = - \frac{\sum_{n'} \mathcal{C}_{n-n'} F_{n'}}{\sum_{n'} \mathcal{D}_{n-n'} F_{n'}} \quad (1.2)$$

where the \mathcal{C}_n and \mathcal{D}_n are the same as before, and the weights F_n are the eigenfunctions of the dispersion equation, associated with the effective wavenumber k_\star .

For monopole scatterers, we have that ($n' = 0$), and the above reduces to equation (1.1). We note that often F_0 is the largest term, which explains why equation (1.1) can give accurate results for non-monopole scatterers, see for example, the numerical results for sound soft (Dirichlet) particles shown in figure 2 in the low-frequency regime. In this same figure, we also see how for sound hard particles (Neumann), which intensively scatter dipole moments, the MC results closely match the formula in equation (1.2), whereas they do not match the formula of the T-matrix for monopole scatterers.

2. Random particulate material

(a) Deterministic scattering from J particles

Here, we summarize some results for multiple scattering of acoustic waves, in the time-harmonic regime, by a collection of J circular cylinders, referred to as particles, with axes aligned

with the z -axis. The centre of the i th particle is identified by $\mathbf{r}_i \in \mathbb{R}^2$ as shown in figure 3 and is assumed to be confined in a region denoted by \mathcal{R}_i . This means that all particles are contained inside the following set:

$$\mathcal{R} := \{\mathbf{r} \in \mathbb{R}^2 : |\mathbf{r}| \leq R\}. \quad (2.1)$$

The propagation of waves in free space is governed by the two-dimensional Helmholtz equation.²

$$\Delta u + k^2 u = 0, \quad (2.2)$$

where $\Delta := \partial_x^2 + \partial_y^2$ is the two-dimensional Laplace operator, and $k \in \mathbb{R}$ is the wavenumber of the homogeneous background. Consider the following basis of the solutions of Helmholtz equation V_n and U_n defined by

$$\begin{cases} U_n(k\mathbf{r}) & := H_n(kr)e^{in\theta} \quad \forall \mathbf{r} \in \mathbb{R}^2 \setminus \{\mathbf{0}\} \\ V_n(k\mathbf{r}) & := J_n(kr)e^{in\theta} \quad \forall \mathbf{r} \in \mathbb{R}^2, \end{cases} \quad (2.3)$$

where (r, θ) are the polar coordinates of \mathbf{r} , i.e. $\mathbf{r} = (r \cos \theta, r \sin \theta)$, J_n are Bessel functions and H_n are Hankel functions, both of the first kind. The specific solutions $V_n(k\mathbf{r})$ have the particularity of being smooth while $U_n(k\mathbf{r})$ have a singularity at the origin and are outgoing solutions.

To analyse acoustic scattering, we follow the same procedure as in [19,34]. Both the incident field u_{inc} and the scattered field u_{sc} are solutions of equation (2.2). We assume that u_{inc} is smooth and regular in the region that covers the particles³, the scattered field has to be a sum of outgoing fields from each particle centred at \mathbf{r}_i , as a result, we can write

$$u_{inc}(\mathbf{r}) = \sum_{n=-\infty}^{+\infty} g_n V_n(k\mathbf{r}), \quad (2.4)$$

$$u_{sc}(\mathbf{r}) = \sum_{i=1}^J \sum_{n=-\infty}^{+\infty} f_n^i U_n(k\mathbf{r} - k\mathbf{r}_i). \quad (2.5)$$

For a known incident wave, its coefficients, $g_n \in \mathbb{C}$, can be calculated via Bessel expansion while the scattering coefficients, $f_n^i \in \mathbb{C}$, are unknowns that can be determined by following the multipole method [35]. The latter leads to the following system of equations:

$$f_n^i = T_n^i \sum_{n'} V_{n'-n}(k\mathbf{r}_i) g_{n'} + T_n^i \sum_{j \neq i} \sum_{n'} U_{n'-n}(k\mathbf{r}_i - \mathbf{r}_j) f_n^j, \quad \forall n \in \mathbb{Z}, \quad \forall i = 1 \dots J, \quad (2.6)$$

where T_n^i is the T-matrix of particle i , which can represent a wide range of particles [36].

To give an example, the expression of a T-matrix of a homogeneous particle with wavenumber k_i , density ρ_i and radius a_i is given by

$$T_n^i = - \frac{\rho_i k J_n'(k a_i) J_n(k a_i) - \rho k_i J_n(k a_i) J_n'(k_i a_i)}{\rho_i k H_n'(k a_i) J_n(k a_i) - \rho k_i H_n(k a_i) J_n'(k_i a_i)}. \quad (2.7)$$

The system of equations (2.6) totally determines the scattering coefficients f_n^i , which allows to solve the scattering problem from the J given particles. However, this result is not very useful in practice for two main reasons: first, the position of the particles is often unknown, and second, there can be a very large number of particles in most industrial applications [37]. The ensemble average over all particle positions, that we summarize below, solves both these problems from the computational standpoint.

²Time evolution of the harmonic waves follows the convention $\text{Re}\{u(\mathbf{r})e^{-i\omega t}\}$.

³This is true for any source which originated from the region outside of where the particles are placed.

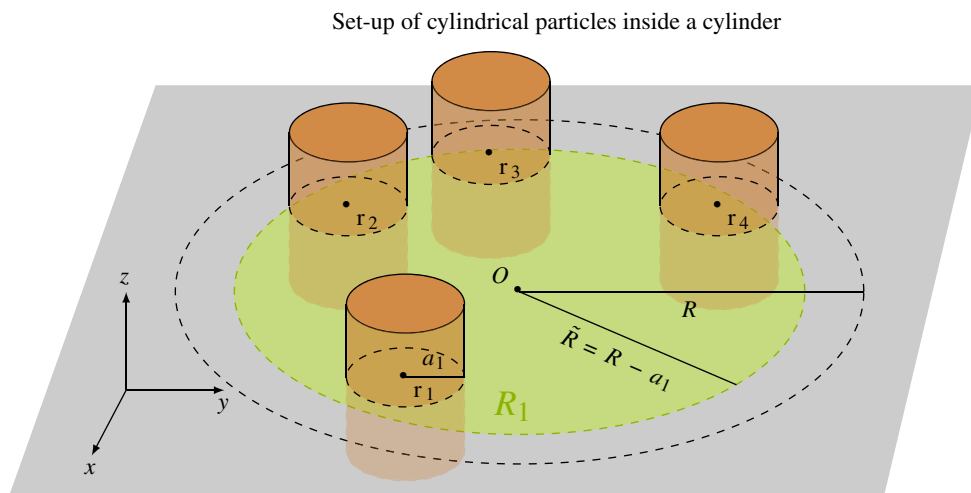


Figure 3. Illustration of a possible configuration of four particles. The particles are cylinders whose axes are aligned with the z -axis. The position $\mathbf{r}_i \in \mathbb{R}^2$ of the i^{th} particle is determined by the intersection of its axis with the plane xOy . The particles are of radius a_i and physically contained in a cylinder of radius R . In this specific example, all the particles have the same radius $a_i = a_1$ and the centres \mathbf{r}_i are therefore confined in the same disc \mathcal{R}_1 shown in green.

(b) Particulate distribution

(i) Single particle distribution

We describe each particle, say particle i , with two random variables: the random variable \mathbf{r}_i , whose values are the possible positions of the centre of particle i in space (\mathbb{R}^2), and the random variable λ_i , which describes all other properties of the particle (radius a_i , density ρ_i , etc.). To set ideas, we will assume that λ_i only describes the radius a_i and ranges in the following set:

$$\mathcal{S} := [A^-, A^+], \quad (2.8)$$

where A^- (resp. A^+) is the minimal (resp. maximal) possible particle radius.

The values (in \mathbb{R}^2) taken by \mathbf{r}_i depend on λ_i . For example, the values of \mathbf{r}_i have to be one radius a_i away from the boundary $\partial\mathcal{R}$, which completely contains all particles (cf. figure 3). In this article, we assume that \mathbf{r}_i is distributed uniformly over the set $\mathcal{R}_i(\lambda_i)$ defined by

$$\mathcal{R}_i := \{\mathbf{r} \in \mathcal{R} : \text{dist}(\mathbf{r}, \partial\mathcal{R}) > a_i\}. \quad (2.9)$$

This assumption translates to

$$p(\mathbf{r}_i | \lambda_i) = \frac{1}{|\mathcal{R}_i|},$$

where $p(\mathbf{r}_i | \lambda_i)$ is the probability distribution of \mathbf{r}_i conditional to λ_i , and $|\mathcal{R}_i|$ is the area of \mathcal{R}_i . Bayes theorem allows to specify the probability distribution $p(\mathbf{r}_i, \lambda_i)$ of the pair of random variables $(\mathbf{r}_i, \lambda_i)$ with respect to the probability $p(\lambda_i)$ of a single particle i to have properties λ_i :

$$p(\mathbf{r}_i, \lambda_i) = p(\mathbf{r}_i | \lambda_i)p(\lambda_i) = \frac{p(\lambda_i)}{|\mathcal{R}_i|}. \quad (2.10)$$

This equation represents the choice of a probability distribution that does not have any preferential position \mathbf{r}_i for the single particle i , which means there is no agglomeration owing to an external force acting on the particles.

(ii) Joint particle distribution

Each particle is described by two random variables $(\lambda_i, \mathbf{r}_i)$, $i = 1, \dots, J$. In general, the particle positions are correlated, for example, no particles can overlap. The most commonly used term to describe inter-particle correlation is the pair correlation g , which satisfies (cf. [38, eqn 8.1.2]):

$$p(\mathbf{r}_1; \mathbf{r}_2 | \lambda_1; \lambda_2) = \frac{g(\mathbf{r}_1, \lambda_1; \mathbf{r}_2, \lambda_2)}{|\mathcal{R}_1| |\mathcal{R}_2|} \frac{J}{J-1}, \quad (2.11)$$

where on the left is the joint law of two-particle positions when their properties are known.

The pair correlation g describes how correlated any two particles are, when the positions and properties of all other particles are unknown. For example, if $g = 1$ for all values of its arguments then both \mathbf{r}_i and \mathbf{r}_j in the above are independent and uniformly distributed over \mathcal{R}_i and \mathcal{R}_j , respectively (in the limit $J \rightarrow \infty$).

Finally, we introduce the density

$$n(\lambda_i) := \frac{J}{|\mathcal{R}_i|} p(\lambda_i) \quad (\text{number of } \lambda_i \text{ type particles per unit volume}). \quad (2.12)$$

Then we derive the following useful relation:

$$p(\mathbf{r}_j, \lambda_j | \mathbf{r}_i, \lambda_i) = \frac{p(\mathbf{r}_j, \lambda_j; \mathbf{r}_i, \lambda_i)}{p(\mathbf{r}_i, \lambda_i)} = |\mathcal{R}_i| p(\lambda_j) p(\mathbf{r}_i; \mathbf{r}_j | \lambda_i; \lambda_j) = \frac{n(\lambda_j)}{J-1} g(\mathbf{r}_i, \mathbf{r}_j), \quad (2.13)$$

where we used equations (2.10)–(2.12).

(iii) The pair correlation

In this article, we consider that the particles have a distribution that is isotropic and homogeneous in space. As a consequence, the pair correlation is of the form $g(\mathbf{r}_i, \lambda_i; \mathbf{r}_j, \lambda_j) = g(|\mathbf{r}_j - \mathbf{r}_i|, \lambda_i, \lambda_j)$. We assume the pair correlation is of the following form:

$$g(r, \lambda_1, \lambda_2) = \begin{cases} 0, & r < a_{12}, \\ 1 + \delta g(r, \lambda_1, \lambda_2), & a_{12} < r < b_{12}, \\ 1, & r > b_{12}, \end{cases} \quad (2.14)$$

where $g(r, \lambda_1, \lambda_2) = 0$ when particles overlap, with a_{12} being the minimum allowed distance between particles of type λ_1 and λ_2 ($a_{12} \geq a_1 + a_2$). This form of the pair correlation moreover assumes that at a certain distance b_{12} from each other, the particles become uncorrelated, that is, $g(r, \lambda_1, \lambda_2) = 1$ for $r > b_{12}$. This assumption will lead to analytic simplifications, as well as being a good approximation for most disordered materials. A typical plot of the pair correlation (see [39,40]) is illustrated in figure 4.

(c) Definition of the effective T-matrix

The expression of the scattered field in equation (2.5) can be simplified after using Graf's addition theorem (equation (A 1),ii) with $\mathbf{x} = k\mathbf{r}$ and $\mathbf{d} = -k\mathbf{r}_i$

$$u_{\text{sc}}(\mathbf{r}) = \sum_{n=-\infty}^{+\infty} \mathfrak{F}_n U_n(k\mathbf{r}), \quad (2.15)$$

$$\mathfrak{F}_n := \sum_{i=1}^J \sum_{n'=-\infty}^{+\infty} V_{n'-n}(-k\mathbf{r}_i) f_{n'}^i. \quad (2.16)$$

Note that equations (2.15) and (2.16) are only valid for $r > R$, nevertheless, this is enough for the definition of the effective T-matrix below. Taking the ensemble average of the equation above, as defined in appendix B, leads to

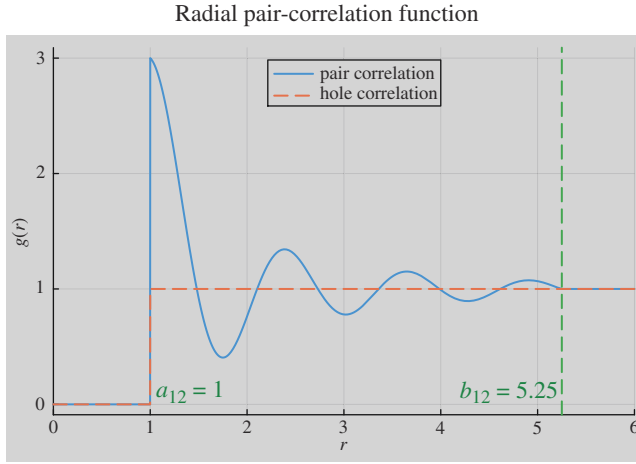


Figure 4. Typical plot of the pair correlation function. The pair-correlation $g(r)$ is zero for $r < a_{12}$ because particles cannot overlap. The local minima (maxima) indicate that there is a distance r from one fixed particle, say at r_1 , where it is less (more) likely to find other particles. Finally, assuming $g(r) = 1$ for $r \geq b_{12}$ means that a particle at r_1 becomes uncorrelated to particles that are further than b_{12} . All variables are dimensionless so that $a_{12} = 1$.

$$\langle u_{\text{sc}}(\mathbf{r}) \rangle = \sum_{n=-\infty}^{+\infty} \langle \mathfrak{F}_n \rangle U_n(k\mathbf{r}), \quad |\mathbf{r}| < R. \quad (2.17)$$

Since the scattering problem is linear with respect to the incident field, $\langle \mathfrak{F}_n \rangle$ depends linearly on the coefficients g_n of the incident field (cf. definition of the incident field u_{inc} equation (2.4)):

$$\langle \mathfrak{F}_n \rangle = \sum_{N=-\infty}^{+\infty} \mathcal{T}_{n,N} g_N \quad (\text{effective T-matrix definition}). \quad (2.18)$$

This relation defines the T-matrix \mathcal{T} of the averaged material that connects the modes of the incident field with the ones of the averaged scattered field. It allows us to describe the scattering from any incident field, provided the coefficients g_n in equation (2.4) are known.

In the specific case when the region where the particles are confined is circular, we have $\mathcal{T}_{n,N} = 0$ if $n \neq N$ (cf. appendix E), so that equation (2.17) becomes

$$\langle u_{\text{sc}}(\mathbf{r}) \rangle = \sum_{n=-\infty}^{+\infty} T_n g_n U_n(k\mathbf{r}), \quad |\mathbf{r}| < R, \quad (2.19)$$

where $T_n := \mathcal{T}_{n,n}$.

Computing $\mathcal{T}_{n,N}$ requires to compute $\langle \mathfrak{F}_n \rangle$. From equations (2.15), (B 1) and (B 3), we obtain

$$\langle \mathfrak{F}_n \rangle = \int_S n(\lambda_1) \int_{\mathcal{R}_1} \sum_{n'} V_{n'-n}(-k\mathbf{r}_1) \langle f_{n'} \rangle(\mathbf{r}_1, \lambda_1) d\mathbf{r}_1 d\lambda_1. \quad (2.20)$$

Here, we used equation (B 7) to substitute $\langle f_n \rangle(\mathbf{r}_1, \lambda_1) = \langle f_n^1 \rangle(\mathbf{r}_1, \lambda_1)$.

The function $\langle f_n \rangle(\mathbf{r}_1, \lambda_1)$ needs to be determined before we can compute $\langle \mathfrak{F}_n \rangle$. In appendix B 2, we show how to obtain the governing equation:

$$\begin{aligned} \langle f_n \rangle(\mathbf{r}_1, \lambda_1) &= T_n(\lambda_1) \sum_{n'} V_{n'-n}(k\mathbf{r}_1) g_{n'} \\ &+ T_n(\lambda_1) \sum_{n'} \int_S n(\lambda_2) \int_{\mathcal{R}_2} U_{n'-n}(k\mathbf{r}_1 - k\mathbf{r}_2) \langle f_{n'} \rangle(\mathbf{r}_1, \lambda_1) g(|\mathbf{r}_1 - \mathbf{r}_2|, \lambda_1 \lambda_2) d\mathbf{r}_2 d\lambda_2, \end{aligned} \quad (2.21)$$

where we also used the simpler pair-correlation given by equation (2.14). Note that equation (2.21) is also valid in the case of non-circular particles, as soon as the probability distribution

of the orientations of any particle in the $(O, \mathbf{x}, \mathbf{y})$ plane is uniform over $[0, 2\pi]$ and independent of all other particles (see [19] for a derivation in the three-dimensional case). Intuitively, the particle averaged over all possible orientations behaves as a circular particle after averaging, and only the diagonal terms $T_n(\lambda_1)$ of its non-diagonal T-matrix contribute to the resulting governing equation.

In the next section, we use the EWM to solve equation (2.21). This method introduced in [19] proved to be successful in the three-dimensional case and provides a closed formula for $\langle f_n \rangle(\mathbf{r}_1, \lambda_1)$. This in turn allows us to compute $\langle \mathfrak{F}_n \rangle$ given by equation (2.20) and reach an explicit formula for $\mathcal{J}_{n,N}$ by specifying $g_n = \delta_{n-N}$ in equation (2.18), where δ is the Kronecker delta:

$$\delta_n = \begin{cases} 1 & \text{if } n = 0 \\ 0 & \text{if } n \neq 0. \end{cases} \quad (2.22)$$

3. The effective wave method

To solve the general governing integral equation (2.21), we use the EWM [19] as summarized below.

Overview of the EWM

The starting point is to assume that there exists $k_\star \in \mathbb{C}$ such that

$$(\Delta + k_\star^2) \langle f_n \rangle(\mathbf{r}_1, \lambda_1) = 0, \quad \lambda_1 \in \mathcal{S}, \quad |\mathbf{r}_1| < R_1. \quad (3.1)$$

This assumption will greatly simplify the governing integral equation (2.21), from which we will be able to determine both k_\star and $\langle f_{n,N} \rangle(\mathbf{r}_1, \lambda_1)$. To summarize, the method has three steps:

- (i) *Separate microstructure and boundary.* The assumption made with equation (3.1) is used in the governing equation (2.21) to derive two separate equations called the *ensemble wave equation* and the *ensemble boundary condition*. The first one only depends on the microstructure of the random material while, in contrast, the second one takes into account the incident field and the shape of the random material, acting much like a boundary condition.
- (ii) *The effective eigensystem.* We decompose $\langle f_{n,N} \rangle(\mathbf{r}_1, \lambda_1)$ in the basis of functions $V_n(k_\star \mathbf{r}_1)$ and substitute the decomposition into the *ensemble wave equation*. The coefficients $\mathbf{F}(\lambda_1)$ of the decomposition are then shown to be the eigenfunctions of an eigensystem whose eigenvalue is k_\star .
- (iii) *The ensemble boundary condition.* To determine the amplitudes of the eigenfunctions $\mathbf{F}(\lambda_1)$, we then use the *ensemble boundary condition*, which takes into account the incident field and the shape of the random material.

(a) Separate microstructure and boundary

We follow the steps described above to determine the solutions $\langle f_n \rangle(\mathbf{r}_1, \lambda_1)$ of equation (2.21). The first step uses equation (3.1), and some algebraic manipulations shown in appendix C.1 to rewrite the governing equation (2.21) into two separate equations:

$$\langle f_n \rangle(\mathbf{r}_1, \lambda_1) + \sum_{n' \in \mathbb{Z}} T_{n'}(\lambda_1) \int_{\mathcal{S}} \left[\frac{J_{n'n}(\mathbf{r}_1)}{k^2 - k_\star^2} - \mathcal{K}_{n'n}(\mathbf{r}_1) \right] \mathbf{n}(\lambda_2) d\lambda_2 = 0 \quad (\text{ensemble wave equation}), \quad (3.2)$$

$$\sum_{n'} V_{n'-n}(k_\star \mathbf{r}_1) g_{n'} + \sum_n \int_{\mathcal{S}} \frac{J_{n'n}(\mathbf{r}_1)}{k^2 - k_\star^2} \mathbf{n}(\lambda_2) d\lambda_2 = 0 \quad (\text{ensemble boundary condition}). \quad (3.3)$$

The terms $\mathcal{J}_{n'n}(\mathbf{r}_1)$, $\mathcal{J}_{n'n}(\mathbf{r}_1)$ and $\mathcal{K}_{n'n}(\mathbf{r}_1)$, respectively, defined in equations (C 6) and (C 3), involve the function $\langle f_{n,N} \rangle(\mathbf{r}_1, \lambda_1)$.

One of the key advantages of splitting the integral equation (2.21) into the two separate equations above is that the ensemble wave equation (3.2) does not depend on the shape of the region \mathcal{R} or the incident wave. As we will see below, the ensemble wave equation (3.2) can be used to determine the effective wavenumber k_\star , which implies that k_\star only depends on the microstructure: the density of the particles $n(\lambda_1)$, their properties provided by the T-matrix $T_n(\lambda_1)$ and the pair correlation g , which explicitly appears in the quantity $\mathcal{K}_{n,n}(\mathbf{r}_1)$ defined in equation (C 3). We further discuss how to interpret k_\star in §4.5.

On the other hand, the ensemble boundary condition (equation (3.3)) acts like a boundary condition and shows how the incident wave and material boundary affect the overall solution.

(b) The effective eigensystem

Since $\langle f_n \rangle(\mathbf{r}_1, \lambda_1)$ satisfies equation (3.1), it can be decomposed into the modes

$$\langle f_n \rangle(\mathbf{r}_1, \lambda_1) = \sum_{n_1} F_{nn_1}(\lambda_1) V_{n_1}(k_\star \mathbf{r}_1), \quad \lambda_1 \in \mathcal{S}, \quad |\mathbf{r}_1| < R_1, \quad (3.4)$$

where V_{n_1} is defined in equation (2.3).

The unknowns k_\star and $F_{nn_1}(\lambda_1)$ can be determined by substituting equation (3.4) into equation (3.2). The details are shown in appendix C2 with the resulting equation being

$$F_{nn_1}(\lambda_1) + \sum_{n'n_2} \delta_{n_2 - n_1 + n' - n} T_n(\lambda_1) \int_{\mathcal{S}} \mathcal{N}_{n'-n}^{12}(k, k_\star) F_{n'n_2}(\lambda_2) n(\lambda_2) d\lambda_2 = 0, \quad (3.5)$$

where δ_n is defined by equation (2.22) and

$$\mathcal{N}_l^{12}(k, k_\star) := 2\pi \frac{N_l(ka_{12}, k_\star a_{12})}{k_\star^2 - k^2} - 2\pi \int_{a_{12}}^{b_{12}} J_l(k_\star r) H_l(kr) \delta g(r) r dr, \quad (3.6)$$

$$N_l(x, y) := x H_l'(x) J_l(y) - y H_l(x) J_l'(y). \quad (3.7)$$

The above is a nonlinear eigenvalue problem, which is why we refer to k_\star as an eigenvalue. After calculating k_\star we can calculate the eigenfunctions $F_{n'n_2}(\lambda_1)$ by solving the linear system of equation (3.5), though, in practice, it is far better to calculate both k_\star and $F_{n'n_2}(\lambda_1)$ using the modal decomposition, as we do in §4.

(c) The ensemble boundary condition

The eigensystem equation (3.5) is not enough to fully determine the F_{nn_1} , for instance, if F_{nn_1} is a solution to the eigensystem then so is αF_{nn_1} for any scalar α .

To fully determine F_{nn_1} , we need to substitute equation (3.4) into the ensemble boundary condition, namely equation (3.3). The details are shown in appendix D, the key results being equations (D5) and (D6), which exploit the symmetry of the region \mathcal{R}_2 , when chosen to be a cylinder. Combining these two equations after setting the radius $R_2 := R - a_2$ finally results in the boundary condition:

$$g_N + \frac{2\pi}{k_\star^2 - k^2} \sum_{n'} \int_{\mathcal{S}} F_{n'(N-n')}(\lambda_2) N_{N-n'}(kR_2, k_\star R_2) n(\lambda_2) d\lambda_2 = 0, \quad (3.8)$$

where N_l is defined by equation (3.6).

4. An effective cylinder

(a) Modal decomposition of the problem

In this section, we exploit the rotational symmetry of the region defined by equation (2.1) in which the particles are contained. Since equation (2.21) is linear with respect to g_n , it can be decomposed into simpler and independent equations: let $\langle f_{n,N} \rangle(\mathbf{r}_1, \lambda_1)$ be the solution when substituting $g_n = \delta_{N-n}$ in equation (2.21), then

$$\begin{aligned} \langle f_{n,N} \rangle(\mathbf{r}_1, \lambda_1) &= T_n(\lambda_1) V_{N-n}(k\mathbf{r}_1) \\ &+ T_n(\lambda_1) \sum_{n'} \int_S n(\lambda_2) \int_{\mathcal{R}_2} U_{n'-n}(k\mathbf{r}_1 - k\mathbf{r}_2) \langle f_{n',N} \rangle(\mathbf{r}_1, \lambda_1) g(|\mathbf{r}_1 - \mathbf{r}_2|, \lambda_1, \lambda_2) d\mathbf{r}_2 d\lambda_2, \end{aligned} \quad (4.1)$$

then we can recover the solution for any incident wave by using

$$\langle f_n \rangle(\mathbf{r}_1, \lambda_1) = \sum_N g_N \langle f_{n,N} \rangle(\mathbf{r}_1, \lambda_1). \quad (4.2)$$

From the three-dimensional version of these effective equations [19], we know that equation (3.5) can be reduced by using symmetry. We show how to do this for the modal decomposition below, with the result being:

$$\langle f_{n,N} \rangle(\mathbf{r}_1, \lambda_1) = \alpha_N F_{n,N}(\lambda_1) V_{N-n}(k_* \mathbf{r}_1), \quad (4.3)$$

where $\alpha_N \in \mathbb{C}$ is some amplitude that is introduced for later convenience. Below is the proof of equation (4.3).

Proof. Using the rotational symmetry of the modal source, we simplify the form of the modal solutions $\langle f_{n,N} \rangle(\mathbf{r}_1, \lambda_1)$. To this end, we denote by \mathbf{R}_ϕ the rotation matrix of angle ϕ and replace \mathbf{r}_1 with $\mathbf{R}_\phi \mathbf{r}_1$ in equation (4.1):

$$\begin{aligned} \langle f_{n,N} \rangle(\mathbf{R}_\phi \mathbf{r}_1, \lambda_1) &= T_n(\lambda_1) V_{N-n}(k\mathbf{R}_\phi \mathbf{r}_1) \\ &+ T_n(\lambda_1) \sum_{n'} \int_S n(\lambda_2) \int_{\mathcal{R}_2} U_{n'-n}(k\mathbf{R}_\phi \mathbf{r}_1 - k\mathbf{R}_\phi \mathbf{r}_2) \langle f_{n',N} \rangle(\mathbf{R}_\phi \mathbf{r}_2, \lambda_2) g(|\mathbf{r}_1 - \mathbf{r}_2|) d\mathbf{r}_2 d\lambda_2, \end{aligned} \quad (4.4)$$

where we changed the integration variable from \mathbf{r}_2 to $\mathbf{R}_\phi \mathbf{r}_2$, which is possible for any rotation as \mathcal{R}_2 is a disc. Then, from equation (2.3) we deduce the property

$$U_n(\mathbf{R}_\phi \mathbf{r}_1) = U_n(\mathbf{r}_1) e^{in\phi} \quad \text{and} \quad V_n(\mathbf{R}_\phi \mathbf{r}_1) = V_n(\mathbf{r}_1) e^{in\phi},$$

using the latter in equation (4.4), and then multiplying both sides of the equation with $e^{-i(N-n)\phi}$ leads to

$$\begin{aligned} \langle f_{n,N} \rangle(\mathbf{R}_\phi \mathbf{r}_1, \lambda_1) e^{-i(N-n)\phi} &= T_n(\lambda_1) V_{N-n}(k\mathbf{r}_1) + \\ T_n(\lambda_1) \sum_{n'} \int_S n(\lambda_2) \int_{\mathcal{R}_2} U_{n'-n}(k\mathbf{r}_1 - k\mathbf{r}_2) e^{-i(N-n)\phi} \langle f_{n',N} \rangle(\mathbf{R}_\phi \mathbf{r}_2, \lambda_2) g(|\mathbf{r}_1 - \mathbf{r}_2|) d\mathbf{r}_2 d\lambda_2. \end{aligned} \quad (4.5)$$

Now note that both $\langle f_{n,N} \rangle(\mathbf{R}_\phi \mathbf{r}_1, \lambda_1) e^{-i(N-n)\phi}$ and $\langle f_{n,N} \rangle(\mathbf{r}_1)$ solve exactly the same integral equation. So by assuming uniqueness, i.e. that there is only one solution to the above, we conclude that

$$\langle f_{n,N} \rangle(\mathbf{r}_1) = \langle f_{n,N} \rangle(\mathbf{R}_\phi \mathbf{r}_1) e^{-i(N-n)\phi}, \quad (4.6)$$

for any \mathbf{r}_1 and ϕ . Let (r_1, θ_1) be the polar coordinates of \mathbf{r}_1 , then, without loss of generality, we then choose $\phi = -\theta_1$, which leads to

$$\langle f_{n,N} \rangle(r_1, \theta_1, \lambda_1) = \langle f_{n,N} \rangle(r_1, 0, \lambda_1) e^{i(N-n)\theta_1}. \quad (4.7)$$

Finally, because $\langle f_{n,N} \rangle(\mathbf{r}_1)$ satisfies a wave equation (3.1), the only possibility for it to satisfy equation (4.7) is to be of the form given in equation (4.3). ■

(b) The modal dispersion equation

We can deduce a simpler effective eigensystem and dispersion equation by using the symmetry equation (4.3). To start we substitute equations (C 8) and (4.3) into the modal decomposition in equation (4.2) to obtain

$$\sum_{n_1} F_{nn_1}(\lambda_1) V_{n_1}(\mathbf{k}_\star \mathbf{r}_1) = \sum_{N_1} \alpha_{N_1} g_{N_1} F_{n, N_1}(\lambda_1) V_{N_1-n}(\mathbf{k}_\star \mathbf{r}_1). \quad (4.8)$$

Then, since V_n form an orthogonal basis of functions,

$$F_{nn_1} = \sum_{N_1} \delta_{N_1-n_1-n} \alpha_{N_1} g_{N_1} F_{n, N_1}. \quad (4.9)$$

To simplify the effective eigensystem equation (3.5), we consider one mode at a time by taking $g_{N_1} = \delta_{N_1-N}$, which used in equation (4.9) implies that we can substitute $F_{nn_1} = \delta_{N-n_1-n} \alpha_N F_{n, N}$ into equation (3.5). The result after some algebraic manipulations is

$$F_{n, N}(\lambda_1) + \sum_{n'} T_n(\lambda_1) \int_S \mathcal{N}_{n'-n}^{12}(k, \mathbf{k}_\star) F_{n', N}(\lambda_2) \mathbf{n}(\lambda_2) d\lambda_2 = 0. \quad (4.10)$$

The above equation is identical to the case of the eigensystem for plane waves [34] and matches also the eigensystems for a single type of particle [12,41] when taking $\mathbf{n}(\lambda) = \delta(\lambda - \lambda_1)$. This result is somewhat expected as the ensemble wave equation (3.2) does not depend on the incident wave and material geometry, which also explains why the modal index N only appears in $F_{n, N}$ in the above.

Instead of solving equation (3.5), it is far simpler to solve the above and then write the general solution in the modal form using equation (4.9). In practice, to solve equation (4.10), we can discretize the integral over S as a set of reals $\{t_1, \dots, t_S\}$. Then define a block vector \mathbf{F} containing the entries $F_n(t_s)$ for $n = -M, -M+1, \dots, M-1, M$, for some finite M , and for $s = 1, \dots, S$, so that the eigensystem becomes

$$(\mathbf{I} + \mathbf{M}) \cdot \mathbf{F} = \mathbf{0}, \quad (4.11)$$

$$\text{where } M_{nn', ss}(k_\star) = T_n(t_s) \mathcal{N}_{n'-n}^{12}(k, \mathbf{k}_\star) \mathbf{n}(t_s). \quad (4.12)$$

The parameter k_\star is then obtained by solving the equation (4.13)

$$\det[\mathbf{I} + \mathbf{M}(k_\star)] = 0. \quad (4.13)$$

Multiple wavenumbers. The dispersion equation (4.10) has infinitely many eigenvalues k_p with $p = 1, 2, \dots$. Consequently, $\langle f_n \rangle(\mathbf{r}_1)$ can more generally be written as a sum over all the eigenvalues k_p and their corresponding eigenfunctions [42], which leads to more accurate solutions. However, only a small difference in comparison with using just the eigenvalue with the smallest imaginary part is observed (cf. [19,41,42] for details). For this reason, and for simplicity, we only account for the one wavenumber k_\star in this article. See figure 5 for a typical distribution of the many eigenvalues of equation (4.10).

(c) The modal ensemble boundary condition

To determine the α_N that appears in equation (4.9), we need to use the ensemble boundary condition. The simplest way to do this is again to take $g_{N_1} = \delta_{N_1-N}$ in equation (4.9) and then substitute the result into equation (3.8) to obtain

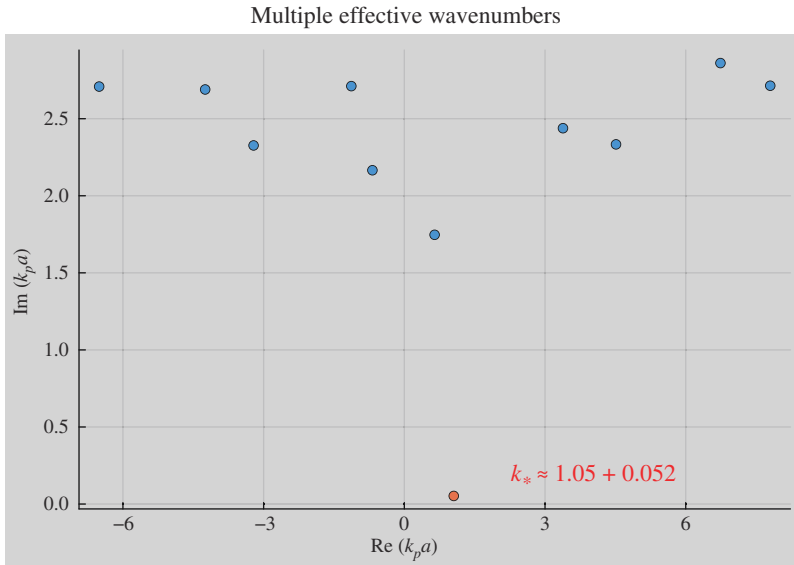


Figure 5. Eleven of the eigenvalues k_p of equation (4.13) for any material filled with sound hard particles of radius $a = 1$ and a particle volume fraction of $n = 0.15$. Here, the frequency is such that $ka = 1$. Note that changing R does not affect the eigenvalues k_p as the dispersion equations (4.10) or (4.11) do not depend on the radius R . k_* corresponds to the one with the smallest imaginary part. The x -axis is the real part, and the y -axis is the imaginary part. The other wavenumbers have a much larger imaginary part leading to evanescent waves inside the random material.

$$1 + \frac{2\pi\alpha_N}{k_*^2 - k^2} \sum_n \int_S F_{n',N}(\lambda_2) N_{N-n}(kR_2, k_*R_2) n(\lambda_2) d\lambda_2 = 0, \quad (4.14)$$

which we can use to determine:

$$\alpha_N = -\frac{k_*^2 - k^2}{2\pi} \left(\sum_n \int_S F_{n',N}(\lambda_2) N_{N-n}(kR_2, k_*R_2) n(\lambda_2) d\lambda_2 \right)^{-1}. \quad (4.15)$$

(d) The effective T-matrix

As discussed in §2(c), the effective T-matrix $\mathcal{J}_{n,N}$ can easily describe the average scattered wave for any incident wave through:

$$\langle \mathfrak{F}_n \rangle = \sum_{N=-\infty}^{+\infty} \mathcal{J}_{n,N} g_N, \quad (4.16)$$

where the $\langle \mathfrak{F}_n \rangle$, given by equation (2.20), are the average coefficients of the waves scattered from the whole cylinder \mathcal{R} . Note the above holds for any choice of g_N and $\mathcal{J}_{n,N}$ does not depend on g_N .

To calculate $\mathcal{J}_{n,N}$, we substitute the modal decomposition given by equation (4.2) into (2.20) to obtain

$$\langle \mathfrak{F}_n \rangle = \sum_N g_N \int_S n(\lambda_1) \int_{\mathcal{R}_1} \sum_n V_{n'-n}(-k\mathbf{r}_1) \langle f_{n',N} \rangle(\mathbf{r}_1, \lambda_1) d\mathbf{r}_1 d\lambda_1. \quad (4.17)$$

Comparing the above with the definition of the effective T-matrix given by equation (4.16), it is clear that

$$\mathcal{J}_{n,N} = \int_S \mathbf{n}(\lambda_1) \int_{\mathcal{R}_1} \sum_{n'} V_{n'-n}(-k\mathbf{r}_1) \langle f_{n',N} \rangle(\mathbf{r}_1, \lambda_1) d\mathbf{r}_1 d\lambda_1. \quad (4.18)$$

To calculate the above, we follow the same steps shown in appendix C. Specifically, we use Green's second identity [equation \(C 4\)](#), the regular expansion [equation \(4.3\)](#) and the orthogonality of the V_n functions to conclude that

$$\mathcal{J}_{n,N} = \delta_{N-n} \frac{2\pi\alpha_n}{k_\star^2 - k^2} \int_S \mathbf{n}(\lambda_1) \sum_{n'} F_{n',n}(\lambda_1) \mathcal{Q}_{n-n}(kR_1, k_\star R_1) d\lambda_1, \quad (4.19)$$

where R_1 is the radius of the disc \mathcal{R}_1 and we defined:

$$\mathcal{Q}_l(x, y) := xJ'_l(x)J_l(y) - yJ_l(x)J'_l(y). \quad (4.20)$$

Finally, we substitute α_n given by [equation \(4.15\)](#), which results in

$$\mathcal{J}_{n,N} = -\delta_{N-n} \frac{\int_S \mathbf{n}(\lambda_1) \sum_{n'} F_{n',n}(\lambda_1) \mathcal{Q}_{n-n}(kR_1, k_\star R_1) d\lambda_1}{\int_S \mathbf{n}(\lambda_1) \sum_{n'} F_{n',n}(\lambda_1) N_{n-n}(kR_1, k_\star R_1) d\lambda_1}. \quad (4.21)$$

We recall that the diagonal terms $\mathcal{J}_{n,n}$ of the effective T-matrix are denoted T_n in this article.

Note that once the effective T-matrix is known, the scattering from any incident field can be computed with [equation \(2.19\)](#) after decomposing the incident field in modes as in [equation \(2.4\)](#). For example, in [figure 6](#), we have plotted the total pressure field $u := u_{\text{inc}} + u_{\text{sc}}$ resulting from an incident plane wave and a point source.

(e) Monopole particles only

The effective T-matrix [equation \(4.21\)](#) resembles the T-matrix for a homogeneous cylinder, see for example [equation \(2.7\)](#). In fact, it is a weighted average of the factors of a homogeneous T-matrix, as explained in §1. From this observation, we see that if the particles are monopole scatterers we obtain a significant simplification.

Let us assume here that the particles scatter only monopole waves, in which case the scattered field given by [equation \(2.5\)](#) becomes

$$\mathbf{u}_{\text{sc}}(\mathbf{r}) = \sum_{i=1}^J f_0^i \mathbf{H}_0(kr - kr_i), \quad (4.22)$$

which leads to $\langle f_{n,N} \rangle(\mathbf{r}_1) = 0$ if $n \neq 0$ and, as a result of [equation \(4.3\)](#), $F_{n,N} = 0$ if $n \neq 0$. Substituting this result into the formula of the effective T-matrix given by [equation \(4.21\)](#), and assuming that the radius R_1 of the region \mathcal{R}_1 is the same for every type of particle λ_1 , we obtain:

$$\mathcal{J}_{n,N}^M = -\delta_{N-n} \frac{kJ'_n(k\tilde{R})J_n(k_\star\tilde{R}) - k_\star J_n(k\tilde{R})J'_n(k_\star\tilde{R})}{kH'_n(k\tilde{R})J_n(k_\star\tilde{R}) - k_\star H_n(k\tilde{R})J'_n(k_\star\tilde{R})} \quad (\text{monopole scatterers}). \quad (4.23)$$

This corresponds to the T-matrix of a homogeneous cylinder of radius $\tilde{R} = R - a$, sound speed $c_\star = \omega/k_\star$ and mass density $\rho_\star = \rho$, where ρ is the density of the host medium (cf. [equation \(2.7\)](#)). The situation of the scattering by monopole particles is illustrated in [figure 7](#).

Average field for two different sources

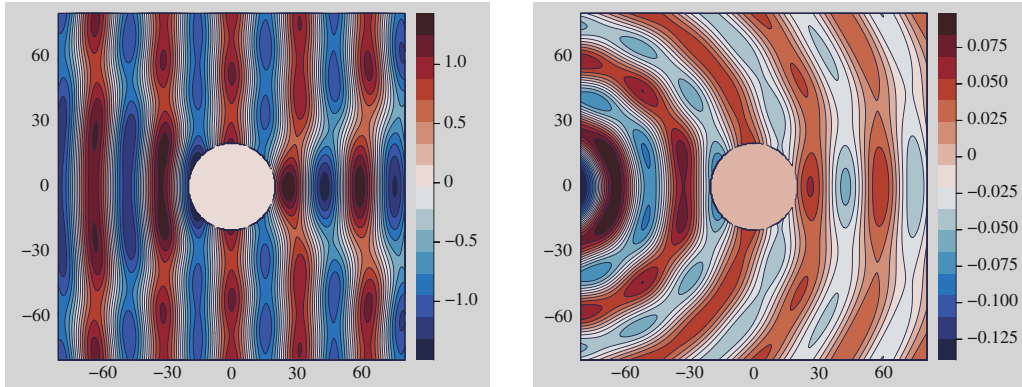


Figure 6. Average pressure field when the incident field is a plane wave (left) and a point source (right). The material is made of sound hard particles of radius $a = 1$ confined in a disc of radius $R = 20$. The particle volume fraction is set to $n = 0.05$. The frequency is such that $ka = 0.1$ and $kR = 2$.

Monte Carlo results: monopole particles

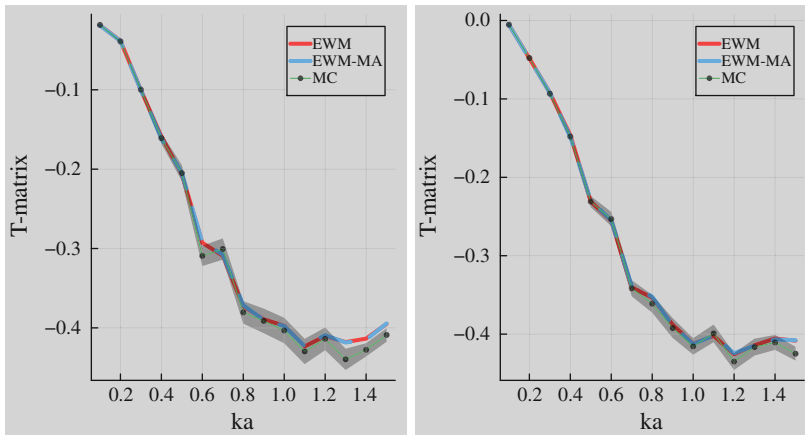


Figure 7. Comparison of various methods to calculate the components T_0 and T_1 of the T-matrix of a cylinder filled with monopole scatterers. The solid red line is our EWM (equation (4.21)), the black points are from the MC method (equation (5.2)) and the dashed blue line is our method when only monopole scattering is accounted for (EWM-MA) (equation (4.23)). In this situation, EWM of course coincides with EWM-MA since the latter corresponds to EWM in the particular case of monopole scatterers. All graphs were generated with particles of radius $a = 1$ inside the cylinder of radius $R = 20$, the volume fraction is set to $n = 0.1$.

5. Numerical results

(a) Data accessibility

The numerical results [43] presented in this section are produced with the open-source software EffectiveTMatrix.jl [44] implemented in Julia. The package source code is also accessible on a GitHub public repository⁴ where the specific script used to generate the data is available⁵.

⁴Repository: <https://github.com/Kevis-Napal/EffectiveTMatrix.jl/tree/1.0.0>

⁵Script: https://github.com/Kevis-Napal/EffectiveTMatrix.jl/blob/1.0.0/examples/RSPA/generate_data.jl

Optimized Monte Carlo simulations

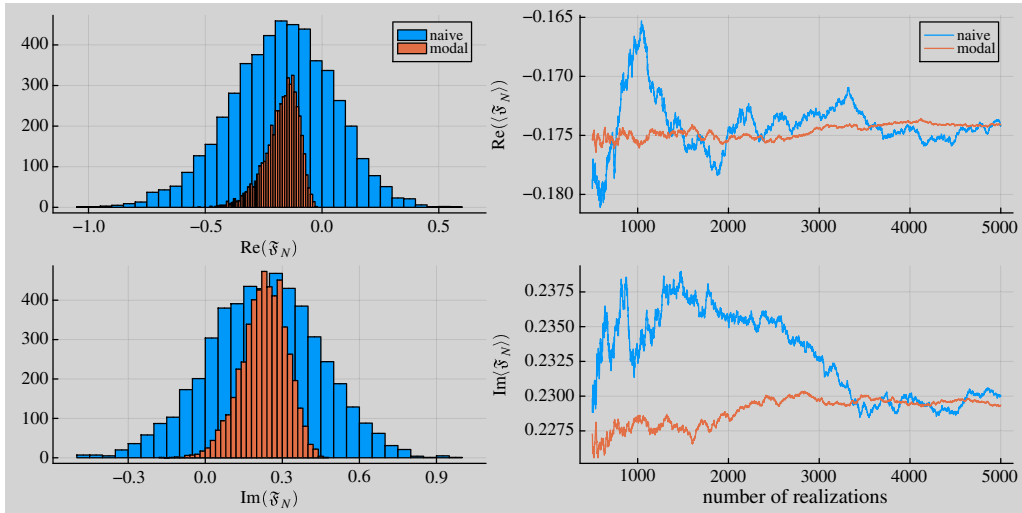


Figure 8. Computation of T_0 using the two different methods given by equations (5.2) (modal) and (5.3) (naive). We computed 5000 realizations of these quantities for different configurations of particles, the plots on the top and bottom, respectively, correspond to the real and imaginary parts of the results. The distribution of the results is reported on the histograms on the left. The plots on the right correspond to the cumulative average of the realizations. Both methods converge to the same limit; however, the modal method converges faster and presents a lower standard deviation of the mean. The simulations were computed with particles of size $a = 1$ constrained in a cylinder of radius $R = 20$, frequency $ka = 1$ and volume fraction of $n = 0.05$.

(b) Optimized Monte Carlo simulations

We use a MC method to validate our theoretical results (equations (4.21) and (4.23)). To develop an efficient MC method, we rely on the following symmetry of the modes:

$$u_{\text{inc}}(\mathbf{r}) = J_N(kr)e^{iN\theta} \implies \langle u_{\text{sc}} \rangle(\mathbf{r}) = T_N H_N(kr)e^{iN\theta}. \quad (5.1)$$

This result is easily obtained from equation (2.19) with the specific choice $g_n = \delta_{n,N}$, which substituted into equation (2.18) leads to

$$T_N = \langle \mathfrak{F}_N \rangle. \quad (5.2)$$

In other words, T_N can be numerically estimated by simulating the waves scattered from one particle configuration at a time by using equation (2.6), and then taking the average of \mathfrak{F}_N defined by equation (2.16) over many different particles configurations.

To illustrate the efficiency of this MC method, we compare it with another method commonly used in the literature [38], which directly computes $\langle u_{\text{sc}} \rangle$. For this second method, we use equation (2.5) to compute $\langle u_{\text{sc}} \rangle(R, 0)$. Then, from equation (5.1), we can also compute T_N with

$$T_N = H_N^{-1}(kR) \langle u_{\text{sc}} \rangle(R, 0). \quad (5.3)$$

The two methods (equations (5.2) and (5.3)) are compared in figure 8. The standard deviation of the mean of the second method is larger than the first one, resulting in a slower convergence. The reason is that equation (5.3), in contrast to equation (5.2), includes all the modes of each scattered field computed for a specific particle configuration:

$$\langle u_{\text{sc}} \rangle(R, 0) = \left\langle \sum_n \mathfrak{F}_n H_n(kR) \right\rangle. \quad (5.4)$$

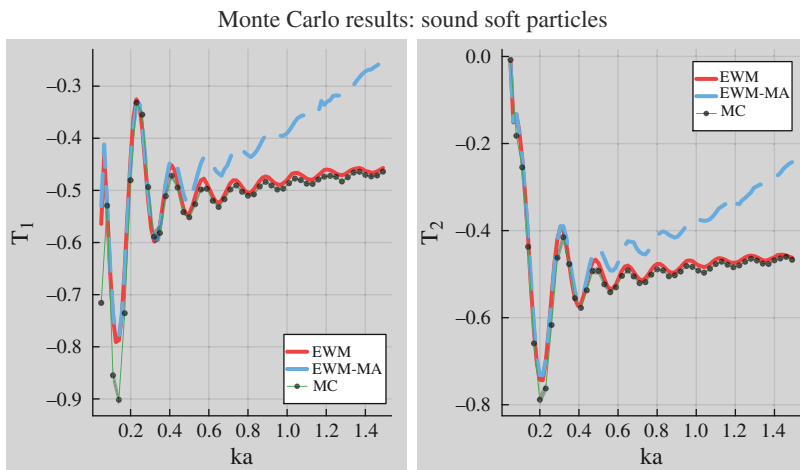


Figure 9. Comparison of various methods to calculate the components T_1 and T_2 of the T-matrix of a cylinder filled with sound-soft particles. The solid red line is our EWM (equation (4.21)), the black points are from the MC method (equation (5.2)) and the dashed blue line is our method when only monopole scattering is accounted for (EWM-MA) (equation (4.23)). The general expression of the effective T-matrix matches the MC results. The EWM-MA method only matches well with the MC for low frequencies. All graphs were generated with a volume fraction $n = 0.05$ of particles with radius $a = 1$ inside the cylinder of radius $R = 20$.

While the terms $n \neq N$ of the sum vanish on average, they significantly contribute to the standard deviation of the mean in equation (5.3).

(c) Validation of the effective waves method

We validate the EWM equation (4.18) against the MC method equation (5.2) for several frequencies ω over an interval Ω , such that the dimensionless variable ka ranges from 0.05 to 1.5. To this end, we define the relative error, averaged over frequencies:

$$\epsilon_n := \frac{1}{|\Omega|} \sum_{\omega \in \Omega} \frac{|T_n^{\text{MC}}(\omega) - T_n^{\text{EWM}}(\omega)|}{|T_n^{\text{MC}}(\omega)|}, \quad (5.5)$$

where $T_n^{\text{MC}}(\omega)$ is obtained following the MC method equation (5.2) and $T_n^{\text{EWM}}(\omega)$ following the EWM equation (4.18). A few plots of $T_n^{\text{MC}}(\omega)$ and $T_n^{\text{EWM}}(\omega)$ are provided in figures 2, 9 and 10. The values of ϵ_0 , ϵ_1 , ϵ_2 , ϵ_3 and ϵ_4 for the cases of sound soft and sound hard particles are reported in tables 1 and 2.

The EWM equation (4.21) gives reliable results for a broad range of frequencies, including high frequencies, provided that the volume fraction is not too high, as shown in figures 2, 7 and 9 the top graph of figure 10 and the first two rows of tables 1 and 2.

Figure 10 shows that the predictions of the EWM for monopole scatterers (equation (4.23)) closely match the MC predictions. So does figure 9 at low frequencies. This is expected, as sound-soft (or Dirichlet) particles are known to behave like monopole scatterers [45] for low frequencies. Figure 9 also shows that as the frequency increases we need to use the EWM that includes higher order modes (or multi-poles) (equation 4.21) to obtain a good match with the MC results. Figure 2 in the introduction also confirms these conclusions.

Finally, the accuracy of the EWM decreases as the volume fraction increases (tables 1 and 2, figure 10). Several parameters influence the precision of the results when increasing the volume fraction. First, a more precise pair correlation function, such as Percus–Yevick, should be used when the volume fraction increases, while we only used the hole correction in our simulations.

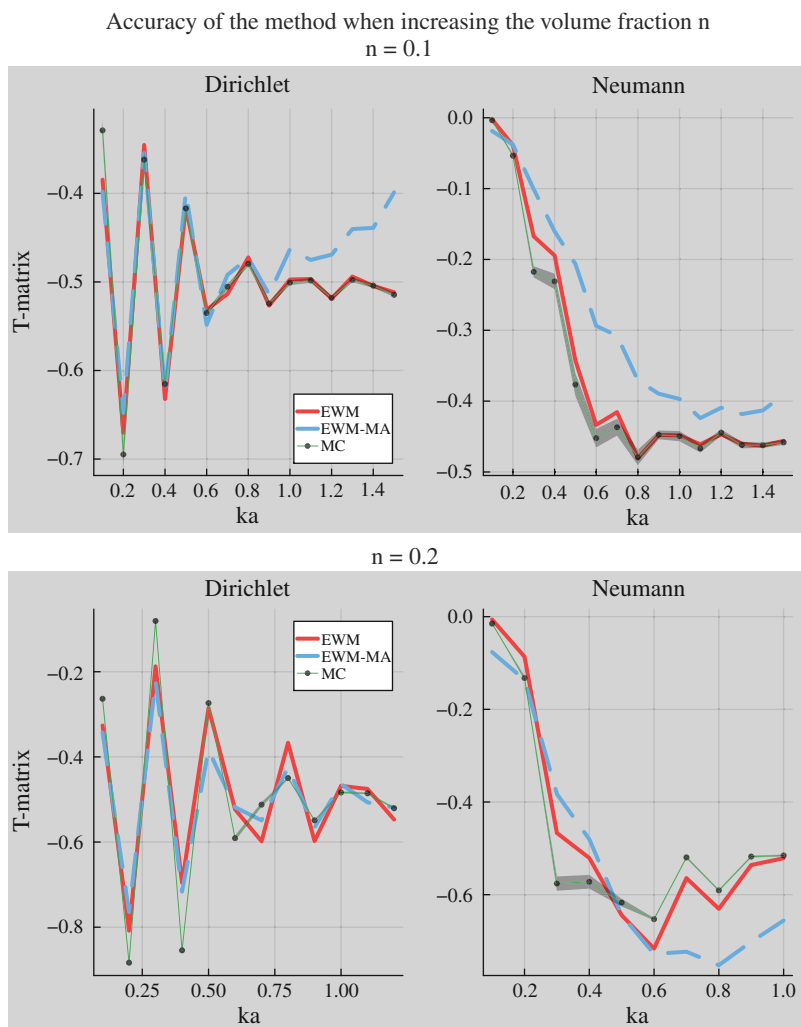


Figure 10. These graphs show similar plots as shown in figure 2 with increased volume fraction, $n = 0.1$ (top) and $n = 0.2$ (bottom). The solid red line is our EWM (equation (4.21)), the black points are from the MC method (equation (5.2)) and the dashed blue line is our method when only monopole scattering is accounted for (EWM-MA) (equation (4.23)). The EWM-MA method is expected to match the MC results only in the case of sound soft particles (Dirichlet) and at low frequencies. Overall, the accuracy of EWM and EWM-MA for predicting MC decreases as the volume fraction increases. All graphs were generated with particles of radius $a = 1$ inside the cylinder of radius $R = 20$.

Table 1. Relative errors ϵ_n are defined by equation (5.5) in the cases of sound hard particles. The particles are of radius 1 and confined in a circular area of radius 20. The computations are made for different volume fractions $n = 0.05, 0.1, 0.2$.

	ϵ_0	ϵ_1	ϵ_2	ϵ_3	ϵ_4
$n = 0.05$	$2.66e^{-2}$	$2.43e^{-2}$	$2.33e^{-2}$	$2.35e^{-2}$	$2.27e^{-2}$
$n = 0.1$	$6.69e^{-2}$	$5.92e^{-2}$	$6.21e^{-2}$	$5.43e^{-2}$	$8.51e^{-2}$
$n = 0.2$	$1.34e^{-1}$	$1.28e^{-1}$	$1.24e^{-1}$	$1.14e^{-1}$	$1.19e^{-1}$

Second, the assumption equation (3.4) is not necessarily valid for densely packed particles, and more effective wavenumbers ($k_p \neq k_*$) are required, such as shown by the decompositions used

Table 2. Relative errors ϵ_n are defined by equation (5.5) in the cases of sound soft particles. The particles are of radius 1 and confined in a circular area of radius 20. The computations are made for different volume fractions $n = 0.05, 0.1, 0.2$.

	ϵ_1	ϵ_2	ϵ_3	ϵ_4
$n = 0.05$	$6.74e^{-2}$	$4.59e^{-2}$	$5.40e^{-2}$	$6.45e^{-2}$
$n = 0.1$	$4.58e^{-2}$	$4.89e^{-2}$	$5.43e^{-2}$	$6.36e^{-2}$
$n = 0.2$	$3.07e^{-1}$	$3.18e^{-1}$	$2.40e^{-1}$	$2.35e^{-1}$

in [19,42]. These multiple effective wavenumbers contribute to a boundary layer that has been neglected in this present work and plays a more important role at higher volume fractions.

6. Conclusion

Main goal. Our main goal was to describe how an incident wave is scattered from a cylinder filled with smaller cylinders, which we have called particles, that are placed in a disordered but correlated way. We describe this correlation through the inter-particle pair correlation, see equation (2.11). The literature so far has focused on plane waves scattered from a halfspace or plate filled with a particulate [17]. There has been at least one paper on solving this scenario, but used an ad hoc method, whereas here everything is deduced from first principles making only two assumptions: such as the QCA [15], and expressing the average field as a sum of effective waves, which has been shown to be the analytic solution [42]. One of the key advantages of describing the scattering from a cylinder with two-dimensional particles is that it is far easier to validate this scenario with direct numerical simulations. Validation is still necessary as the theory requires the use of QCA, whose level of accuracy has not been thoroughly investigated yet. Additionally, confirming this scenario also supports the accuracy of the predicted effective wavenumbers for any material geometry [19].

Modal scattering. We used this method to simplify both the theoretical and MC simulations. By leveraging all present symmetries, we solved for each polar mode of the incident wave separately, which allowed us to streamline the validation process for this work. This simple, but effective technique, leads us to an effective T-matrix given by equation (4.21) that can be used to calculate the average scattered wave from any incident wave, see §3 for a brief overview. We note that we were able to describe the scattered field without calculating the average transmitted field. In future work, this may be interesting to do, for example, to clearly identify when different effective wavenumbers are excited [17].

Effective T-matrix. The result of our theoretical work is summarized by the T-matrix equation (4.21). Beyond using just QCA, to calculate this T-matrix, we also assumed that only one effective wavenumber k_\star is excited. This is true for a wide range of parameters, but it is not always the case. In particular, it appears that very strong scattering at moderate frequencies can trigger more than one effective wavenumber to be excited [17,19,41]. One possible extension to our work is to include the effect of more than one effective wavenumber.

Monopole scatterers. One surprising result is that if the particles only scatter monopole waves, then the effective T-matrix greatly simplifies and becomes equation (4.23). This form is exactly the same as the T-matrix for a homogenous cylinder, one with constant material parameters. We hypothesize that any material filled with monopole scatterers would, on average, respond like a homogeneous material. Monopole scatterers are a good approximation for many types of resonant particles [31]. Figure 9 compares the results for the monopole scattering approximation with MC results for sound-soft particles, which does not assume the particles scatter like monopoles.

Monte Carlo. Beyond deducing an effective T-matrix for a particulate cylinder, we also developed an efficient MC method, which matched our theoretical predictions very accurately (see figures 2 and 9). Our numerical validation was for a broad frequency range, but we did not cover a broad range of parameters. Doing this would be valuable future work and could help clearly identify the limits of QCA and different approximations for the inter-particle pair-correlation.

A prototype for new materials. The setting we deduce is the ideal case to test new disordered particulates. That is, to use exotic inter-particle pair-correlation to achieve effects such as band gaps, or impedance matching. The scenario of a cylinder filled with two-dimensional particles is ideal for testing new types of particles, and inter-particle pair-correlations, because they can be easily validated with MC methods. When designing new materials with exotic responses, and stretching the limits of the theory, we need to have a way to validate those predictions. This article provides such a framework that we recommend for the advancement of innovation in material designs.

Ethics. This work did not require ethical approval from a human subject or animal welfare committee.

Data accessibility. The data presented are openly available in ‘Dataset: Effective T-matrix of a cylinder filled with a random 2D particulate’ at [43]. The data are produced with the open-source software ‘EffectiveTMatrix.jl: A Julia library for computing the effective T-matrix of a random particulate sphere or cylinder’ available at <https://doi.org/10.5281/zenodo.10529120> [44].

Declaration of AI use. We have not used AI-assisted technologies in creating this article.

Authors’ contributions. K.K.N.: conceptualization, formal analysis, investigation, methodology, project administration, software, validation, writing—original draft, writing—review and editing; P.S.P.: conceptualization, formal analysis, investigation, writing—original draft, writing—review and editing; A.L.G.: conceptualization, formal analysis, investigation, writing—original draft, writing—review and editing. All authors gave final approval for publication and agreed to be held accountable for the work performed therein.

Conflict of interest declaration. We declare we have no competing interests.

Funding. Kevissh Napal and Artur Gower gratefully acknowledge support from EPSRC (EP/V012436/1). Paulo Piva gratefully acknowledges funding from a Case studentship with Johnson Matthey.

Appendix A. Bessel functions and translation matrices

Given two points $\mathbf{x}, \mathbf{y} \in \mathbb{R}^2$, we have the following identities where $\mathbf{d} = \mathbf{y} - \mathbf{x}$

$$\left\{ \begin{array}{l} \text{(i)} \quad V_n(\mathbf{y}) = \sum_{n'=-\infty}^{+\infty} V_{n-n'}(\mathbf{d})V_{n'}(\mathbf{x}), \quad \text{for all } \mathbf{x}, \mathbf{d} \in \mathbb{R}^2 \\ \text{(ii)} \quad U_n(\mathbf{y}) = \sum_{n'=-\infty}^{+\infty} V_{n-n'}(\mathbf{d})U_{n'}(\mathbf{x}), \quad \text{for all } |\mathbf{x}| > |\mathbf{d}| \\ \text{(iii)} \quad U_n(\mathbf{y}) = \sum_{n'=-\infty}^{+\infty} U_{n-n'}(\mathbf{d})V_{n'}(\mathbf{x}), \quad \text{for all } |\mathbf{x}| < |\mathbf{d}|. \end{array} \right. \quad (\text{A } 1)$$

The above formulas are direct consequences of Graf’s theorem (see [35, Th. 2.11–2.12] for instance).

Appendix B. Ensemble averaging

B.1. Definitions

Here we give a brief overview of ensemble averaging so that this article is more self-contained. For more details, see [19,35] and the references within. To simplify computations, we represent one particle configurations with:

$$\Lambda = \mathbf{r}_1, \lambda_1 \dots \mathbf{r}_J, \lambda_J, \quad \Lambda^{(1)} = \mathbf{r}_2, \lambda_2 \dots \mathbf{r}_J, \lambda_J,$$

$$\Lambda^{(1,j)} = \mathbf{r}_2, \lambda_2, \dots, \mathbf{r}_{j-1}, \lambda_{j-1}, \mathbf{r}_{j+1}, \lambda_{j+1}, \dots, \mathbf{r}_J, \lambda_J.$$

Using these definitions, we define the ensemble average, and conditional ensemble averages, of a quantity A , which can depend on the positions and properties of all the particles, as

$$\langle A \rangle := \int A(\Lambda) p(\Lambda) d\Lambda \quad \langle A \rangle(\mathbf{r}_i, \lambda_i) := \int A(\Lambda) p(\Lambda^{(i)} | \mathbf{r}_i, \lambda_i) d\Lambda^{(i)}, \quad (\text{B } 1)$$

$$\langle A \rangle(\mathbf{r}_i, \lambda_i; \mathbf{r}_j, \lambda_j) := \int A(\Lambda) p(\Lambda^{(i,j)} | \mathbf{r}_i, \lambda_i; \mathbf{r}_j, \lambda_j) d\Lambda^{(i,j)}, \quad (\text{B } 2)$$

where the domain of integration for Λ is over all possible particle positions and properties. The term $\langle A \rangle(\mathbf{r}_i, \lambda_i; \mathbf{r}_j, \lambda_j)$ is the ensemble average of A conditional to $(\mathbf{r}_1, \lambda_1, \mathbf{r}_2, \lambda_2)$.

Taking an ensemble average defined by [equation \(B 1\)](#) on both sides of [equation \(2.16\)](#) leads to

$$\begin{aligned} \langle \mathfrak{F}_n \rangle &= \sum_{i=1}^J \sum_{n'=-\infty}^{+\infty} \int (-1)^{n-n'} V_{n-n'}(k\mathbf{r}_i) \langle f_n^i \rangle(\mathbf{r}_i, \lambda_i) p(\mathbf{r}_i, \lambda_i) d\mathbf{r}_i d\lambda_i \\ &= J \sum_{n'=-\infty}^{+\infty} \int (-1)^{n-n'} V_{n-n'}(k\mathbf{r}_1) \langle f_n^1 \rangle(\mathbf{r}_1, \lambda_1) p(\mathbf{r}_1, \lambda_1) d\mathbf{r}_1 d\lambda_1 \end{aligned} \quad (\text{B } 3)$$

where we used the definition of conditional probability: $p(\Lambda) = p(\mathbf{r}_i, \lambda_i) p(\Lambda^{(i)})$, the definition of conditional average as in [equation \(B 2\)](#) to introduce the term $\langle f_n^i \rangle(\mathbf{r}_i, \lambda_i)$, and that particles are indistinguishable.⁶ Finally, using [equations \(2.10\)](#) and [\(2.12\)](#) leads [equation \(B 3\)](#) to formula [\(2.18\)](#).

B.2. Average governing equation

Here we briefly show how to reach the averaging governing equation by using just one assumption, the QCA. For more details, see [\[19\]](#).

Taking the conditional average, defined by [equation \(B 1\)₂](#), of [equation \(2.5\)](#) with $i = 1$ gives

$$\begin{aligned} \langle f_n^1 \rangle(\mathbf{r}_1, \lambda_1) &= T_n(\lambda_1) \sum_{n'} V_{n'-n}(k\mathbf{r}_1) g_{n'} \\ &+ T_n(\lambda_1) \sum_{j \neq 1} \sum_{n'} \int U_{n'-n}(k\mathbf{r}_1 - k\mathbf{r}_j) \langle f_n^j \rangle(\mathbf{r}_1, \lambda_1) p(\Lambda^{(1)} | \mathbf{r}_1, \lambda_1) d\Lambda^{(1)}. \end{aligned} \quad (\text{B } 4)$$

We can simplify the above by using the definition of the conditional average defined by [equation \(B 2\)](#) of $f_n^j(\mathbf{r}_1, \lambda_1; \mathbf{r}_j, \lambda_j)$, using [equation \(2.12\)](#), and that particles are indistinguishable to obtain

$$\begin{aligned} \langle f_n^1 \rangle(\mathbf{r}_1, \lambda_1) &= T_n(\lambda_1) \sum_{n'} V_{n'-n}(k\mathbf{r}_1) g_{n'} \\ &+ T_n(\lambda_1) \sum_{n'} \int_{\mathcal{R}_2} n(\lambda_2) \int_{\mathcal{R}_2} U_{n'-n}(k\mathbf{r}_1 - k\mathbf{r}_2) \langle f_n^2 \rangle(\mathbf{r}_2, \lambda_2, \mathbf{r}_1, \lambda_1) g(\mathbf{r}_1, \lambda_1; \mathbf{r}_2, \lambda_2) d\mathbf{r}_2 d\lambda_2. \end{aligned} \quad (\text{B } 5)$$

However, this equation is not a closed-form equation for $\langle f_n^1 \rangle(\mathbf{r}_1, \lambda_1)$, and an extra assumption is required to proceed further.

A standard solution found in the literature to tackle the problem mentioned above is to use the QCA, which is a standard closure approximation [\[46\]](#). It is stated as follows:

$$\langle f_n^2 \rangle(\mathbf{r}_1, \lambda_1; \mathbf{r}_2, \lambda_2) \approx \langle f_n^2 \rangle(\mathbf{r}_2, \lambda_2), \quad |\mathbf{r}_1 - \mathbf{r}_2| \geq a_{12} \quad (\text{QCA}). \quad (\text{B } 6)$$

See [\[34\]](#) for a brief discussion on this approximation.

⁶Said in another way, the variables of integration \mathbf{r}_i and λ_i are just dummy variables which can be all changed to \mathbf{r}_1 and λ_1 .

Finally, we use that particles are indistinguishable, which implies that $\langle f_n^1 \rangle(\mathbf{r}_1, \lambda_1) = \langle f_n^2 \rangle(\mathbf{r}_2, \lambda_2)$ when $\mathbf{r}_1 = \mathbf{r}_2$ and $\lambda_1 = \lambda_2$ to substitute

$$\langle f_n^2 \rangle(\mathbf{r}_2, \lambda_2) = \langle f_n \rangle(\mathbf{r}_2, \lambda_2) \quad \text{and} \quad \langle f_n^1 \rangle(\mathbf{r}_1, \lambda_1) = \langle f_n \rangle(\mathbf{r}_1, \lambda_1), \quad (\text{B } 7)$$

into equation (B 5), which together with QCA given by equation (B 6) leads to the average governing equation (2.19).

Appendix C. The effective waves method

C.1. Derivation of two ensemble equations

Here we show how to use the effective wave assumption to rewrite the governing equation (4.1) into two separate equations: the effective wave equation and the effective boundary condition. To achieve this, we define for $\mathbf{y} \in \mathcal{R}$ and $a > 0$ the set

$$D(\mathbf{y}, a) := \{\mathbf{x} \in \mathcal{R} : |\mathbf{x} - \mathbf{y}| \leq a\}.$$

Using the decomposition of the pair correlation function given in equation (2.13), we split the domain of integration in the governing equation (2.19) into two integrals: one over $D(\mathbf{r}_1, a_{12})$, another one over $\mathcal{R}_2 \setminus D(\mathbf{r}_1, a_{12})$ in the form

$$\begin{aligned} \langle f_n \rangle(\mathbf{r}_1, \lambda_1) &= T_n(\lambda_1) \sum_{n'} V_{N-n}(\mathbf{kr}_1) g_{n'} + T_n(\lambda_1) \sum_{n'} \int_S \mathbf{n}(\lambda_2) \int_{\mathcal{R}_2 \setminus D(\mathbf{r}_1, a_{12})} U_{n'-n}(\mathbf{kr}_1 - \mathbf{kr}_2) \langle f_{n'} \rangle(\mathbf{r}_2, \lambda_2) d\mathbf{r}_2 d\lambda_2 \\ &+ T_n(\lambda_1) \sum_{n'} \int_S \mathbf{n}(\lambda_2) \int_{D(\mathbf{r}_1, a_{12}, b_{12})} U_{n'-n}(\mathbf{kr}_1 - \mathbf{kr}_2) \langle f_{n'} \rangle(\mathbf{r}_2, \lambda_2) \delta g(|\mathbf{r}_1 - \mathbf{r}_2|, \lambda_1, \lambda_2) d\mathbf{r}_2 d\lambda_2, \end{aligned} \quad (\text{C } 1)$$

where $D(\mathbf{r}_1, a_{12}, b_{12}) := D(\mathbf{r}_1, b_{12}) \setminus D(\mathbf{r}_1, a_{12})$ and the annulus $D(\mathbf{r}_1, a_{12}, b_{12})$ is completely contained within \mathcal{R}_2 when

$$\text{dist}(\mathbf{r}_1, \partial\mathcal{R}_2) \geq b_{12}. \quad (\text{C } 2)$$

In this section, and in this article, we only solve equation (4.1) for \mathbf{r}_1 that satisfies the above. This avoids the boundary layer [41,42], which greatly complicates the solution and is only needed when there is a large particle volume fraction, moderate frequencies and strongly scattering particles.

The last integral in equation (C 1) can be simplified by changing the variable of integration to $\mathbf{r} = \mathbf{r}_2 - \mathbf{r}_1$, which leads to the integral

$$\mathcal{K}_{n'n}(\mathbf{r}_1, \lambda_2) := \int_{D(\mathbf{0}, a_{12}, b_{12})} U_{n'-n}(-\mathbf{kr}) \langle f_{n'} \rangle(\mathbf{r} + \mathbf{r}_1, \lambda_2) \delta g(\mathbf{r}, \lambda_1, \lambda_2) d\mathbf{r}. \quad (\text{C } 3)$$

The first integral over \mathbf{r}_2 in equation (C 1) can be further simplified by using Green's theorem to replace the volume integral over $\mathcal{R}_2 \setminus D(\mathbf{r}_1, a_{12})$ by surface integrals: given any two function smooth functions u, v which satisfy

$\Delta u(\mathbf{r}) + k_\star u(\mathbf{r}) = 0$ and $\Delta v(\mathbf{r}) + kv(\mathbf{r}) = 0$, over a set Ω we have that

$$(k^2 - k_\star^2) \int_\Omega uv d\mathbf{r} = \int_\Omega (\Delta uv - u\Delta v) d\mathbf{r} = \int_{\partial\Omega} (\partial_\nu uv - u\partial_\nu v) ds(\mathbf{r}). \quad (\text{C } 4)$$

With $u(\mathbf{r}_2)$ substituted for $\langle f_{n',N} \rangle(\mathbf{r}_2, \lambda_2)$ and $v(\mathbf{r}_2)$ substituted for $U_{n'-n}(\mathbf{kr}_1 - \mathbf{kr}_2)$, we can use the above to deduce:

$$\int_{\mathcal{R}_2 \setminus D(\mathbf{r}_1, a_{12})} U_{n'-n}(\mathbf{kr}_1 - \mathbf{kr}_2) \langle f_{n'} \rangle(\mathbf{r}_2, \lambda_2) d\mathbf{r}_2 = \frac{\mathcal{J}_{n'n}(\mathbf{r}_1) - \mathcal{J}_{n'n}(\mathbf{r}_1)}{k^2 - k_\star^2}, \quad (\text{C } 5)$$

where we defined

$$\begin{aligned} \mathcal{J}_{n'n}(\mathbf{r}_1) &:= \int_{\partial\mathcal{R}_2} \mathcal{U}_{n'-n}(k\mathbf{r}_1 - k\mathbf{r}_2) \frac{\partial \langle f_n \rangle(\mathbf{r}_2, \lambda_2)}{\partial \mathbf{v}_2} - \frac{\partial \mathcal{U}_{n'-n}(k\mathbf{r}_1 - k\mathbf{r}_2)}{\partial \mathbf{v}_2} \langle f_n \rangle(\mathbf{r}_2, \lambda_2) dA_2, \\ \mathcal{J}_{n'n}(\mathbf{r}_1) &:= \int_{\partial D(\mathbf{0}, a_{12})} \mathcal{U}_{n'-n}(-k\mathbf{r}) \frac{\partial \langle f_n \rangle(\mathbf{r} + \mathbf{r}_1, \lambda_2)}{\partial \mathbf{v}} - \frac{\partial \mathcal{U}_{n'-n}(-k\mathbf{r})}{\partial \mathbf{v}} \langle f_n \rangle(\mathbf{r} + \mathbf{r}_1, \lambda_2) dA. \end{aligned} \quad (\text{C } 6)$$

Finally, substituting equations (C 3) and (C 5) into the governing equation (2.19) gives

$$\begin{aligned} \langle f_n \rangle(\mathbf{r}_1, \lambda_1) &= \mathcal{T}_n(\lambda_1) \sum_n \mathcal{V}_{n'-n}(k\mathbf{r}_1) \mathcal{g}_{n'} \\ &+ \sum_{n'} \mathcal{T}_n(\lambda_1) \int_S \left[\frac{\mathcal{J}_{n'n}(\mathbf{r}_1) - \mathcal{J}_{n'n}(\mathbf{r}_1)}{k^2 - k_\star^2} + \mathcal{K}_{n'n}(\mathbf{r}_1) \right] \mathbf{n}(\lambda_2) d\lambda_2. \end{aligned} \quad (\text{C } 7)$$

The above now can be split into two separate equations by noting that the functions $\langle f_n \rangle(\mathbf{r}_1)$, $\mathcal{J}_{n'n}(\mathbf{r}_1)$ and $\mathcal{K}_{n'n}(\mathbf{r}_1)$ satisfy the wave equation with wavenumber k_\star , while $\mathcal{V}_n(k\mathbf{r}_1)$ and $\mathcal{J}_{n'n}(\mathbf{r}_1)$ satisfy the wave equation with wavenumber k . Since solutions of the Helmholtz equation with different wavenumbers are independent, see [19] for details, equation (C 7) can be split into the ensemble wave equation (3.2) containing the terms with wavenumber k_\star and the ensemble boundary condition (equation (3.3)) containing the terms with wavenumber k .

C.2. The effective eigensystem

Here, we deduce a general eigensystem that can be used to determine the effective wavenumber k_\star and write $\langle f_n \rangle(\mathbf{r}_1, \lambda_1)$ in terms of eigenfunctions.

Since $\langle f_n \rangle(\mathbf{r}_1, \lambda_1)$ satisfies the wave equation (3.1), it can be decomposed into the modes

$$\langle f_n \rangle(\mathbf{r}_1, \lambda_1) = \sum_{n_1} F_{nn_1}(\lambda_1) \mathcal{V}_{n_1}(k_\star \mathbf{r}_1), \quad (\text{C } 8)$$

where \mathcal{V}_{n_1} is defined in equation (2.3).

The unknowns k_\star and $F_{nn_1}(\lambda_1)$ can be determined by substituting equation (C 8) into (3.2), which requires the term

$$\langle f_n \rangle(\mathbf{r} + \mathbf{r}_1, \lambda_2) = \sum_{n_1 n_2} F_{nn_1}(\lambda_2) \mathcal{V}_{n_1 - n_2}(k_\star \mathbf{r}) \mathcal{V}_{n_2}(k_\star \mathbf{r}_1), \quad (\text{C } 9)$$

where the right side is a result of using Graf's addition theorem (equation (A 1), i) in (3.4).

By substituting equation (C 9) in $\mathcal{K}_{n'n}(\mathbf{r}_1)$ (C 3), we can use the orthogonality of the cylindrical Bessel functions to remove the sum over n_2 , because only the cases $(n_1 - n_2) = (n - n')$ are non-zero.

Likewise, we can perform the same simplification by substituting equation (C 9) in $\mathcal{J}_{n'n}(\mathbf{r}_1)$ (C 6).

The simplifications result in

$$\begin{aligned} \mathcal{K}_{n'n}(\mathbf{r}_1) &= 2\pi \mathcal{W}_{n'-n}(k, k_\star) \sum_{n_1} F_{n'n_1}(\lambda_2) \mathcal{V}_{n_1 + n' - n}(k_\star \mathbf{r}_1) \mathcal{J}_{n'n}(\mathbf{r}_1) \\ &= -2\pi \mathcal{N}_{n'-n}(ka_{12}, k_\star a_{12}) \sum_{n_1} F_{n'n_1}(\lambda_2) \mathcal{V}_{n_1 + n' - n}(k_\star \mathbf{r}_1), \end{aligned} \quad (\text{C } 10)$$

where we introduced the notations

$$\mathcal{W}_l(k, k_\star) := \int_{a_{12}}^{b_{12}} \mathcal{H}_l(kr) \mathcal{J}_l(k_\star r) \delta g(r, \lambda_1, \lambda_2) r dr, \quad \mathcal{N}_l(x, y) := x \mathcal{H}'_l(x) \mathcal{J}_l(y) - y \mathcal{H}_l(x) \mathcal{J}'_l(y). \quad (\text{C } 11)$$

Finally, substituting equation (C 10) in the ensemble wave equation (3.2), and again using the orthogonality of the cylindrical Bessel functions, we reach equation (3.5) where the following term appears:

$$\mathcal{N}_l^{12}(k, k_\star) = 2\pi \frac{\mathcal{N}_l(ka_{12}, k_\star a_{12})}{k_\star^2 - k^2} - 2\pi \mathcal{W}_l(k, k_\star). \quad (\text{C } 12)$$

Appendix D. Boundary condition for effective waves

The eigensystem equation (3.5) is not enough to fully determine the F_{nm} , to do so we need to substitute equation (3.4) into the ensemble boundary condition equation (3.3). To achieve this, the first step is to use Graf's addition theorem (equation (A 1), iii) with $\mathbf{x} = \mathbf{r}_1$ and $\mathbf{y} = -\mathbf{r}_2$ to obtain

$$U_{n'-n}(k\mathbf{r}_1 - k\mathbf{r}_2) = \sum_{n_3} V_{n_3}(k\mathbf{r}_1) U_{n'-n-n_3}(-k\mathbf{r}_2) = \sum_{n_2} V_{n_2-n+n'}(k\mathbf{r}_1) U_{-n_2}(-k\mathbf{r}_2), \quad (\text{D } 1)$$

where we used the change of variable $n_2 = n + n_3 - n'$, and that $|\mathbf{r}_1| \ll |\mathbf{r}_2|$ because for $\mathcal{J}_{n'n}$ the variable \mathbf{r}_2 is on the boundary $\partial\mathcal{R}_2$, whereas \mathbf{r}_1 satisfies equation (C 2). Substituting equation (3.4) in $\mathcal{J}_{n'n}$ defined by equation (C 6) and using the above equation (D 1) gives

$$\mathcal{J}_{n'n}(\mathbf{r}_1) = \sum_{n_2 n_1} F_{n'n_1}(\lambda_2) \mathcal{B}_{n_1 n_2} V_{n_2-n+n'}(k\mathbf{r}_1), \quad (\text{D } 2)$$

where

$$\mathcal{B}_{n_1 n_2} = (-1)^{n_2} \int_{\partial\mathcal{R}_2} \left[U_{-n_2}(k\mathbf{r}_2) \frac{\partial V_{n_1}(k_\star \mathbf{r}_2)}{\partial \nu_2} - \frac{\partial U_{-n_2}(k\mathbf{r}_2)}{\partial \nu_2} V_{n_1}(k_\star \mathbf{r}_2) \right] dA_2, \quad (\text{D } 3)$$

then substituting equation (D 2) in (3.3) leads to

$$\sum_{n'} V_{n'-n}(k\mathbf{r}_1) \mathcal{G}_{n'} + \sum_{n_2 n_1} \int_{\mathcal{S}} F_{n'n_1}(\lambda_2) V_{n_2-n+n'}(k\mathbf{r}_1) \frac{\mathcal{B}_{n_1 n_2}}{k^2 - k_\star^2} \mathbf{n}(\lambda_2) d\lambda_2 = 0. \quad (\text{D } 4)$$

We can further simplify the above by using the orthogonality of the functions V_n to obtain

$$\mathcal{G}_N + \sum_{n_1} \int_{\mathcal{S}} F_{n'n_1}(\lambda_2) \frac{\mathcal{B}_{n_1(N-n')}}{k^2 - k_\star^2} \mathbf{n}(\lambda_2) d\lambda_2 = 0, \quad (\text{D } 5)$$

which holds for every N .

When all particles are in a disk, then $\partial\mathcal{R}_2$ is a circle and the above simplifies. This is the only case we completely resolve in this article. Let R_2 be the radius of the disk \mathcal{R}_2 , then $n_2 = n_1$ in equation (D 3), which reduces to

$$\mathcal{B}_{n_1 n_2} = -2\pi \delta_{n_1 - n_2} N_{n_1}(kR_2, k_\star R_2), \quad (\text{D } 6)$$

where N_{n_1} is defined by equation (C 11). Substituting this into equation (D 5) leads to (3.8).

Appendix E. Elementary proof that the effective T-matrix is diagonal

We provide an elementary proof that \mathcal{T} is diagonal when the particles are confined in a disk of radius R . To this end, we consider the scattering from the modal source u_{inc}^N obtained for $\mathbf{g}_n = \delta_{n-N}$:

The notation $\mathfrak{F}_{n,N}$ is the corresponding \mathfrak{F}_n to the specific incident field with $\mathbf{g}_n = \delta_{n-N}$ (compare with equation (2.16)). We then denote by $f_{n,N}^i(\sigma)$ the resulting solution of equation (2.5) for the specific configuration $\sigma = \mathbf{r}_1, \dots, \mathbf{r}_J$. The rotation by angle ϕ of the particles $\mathbf{r}_1, \dots, \mathbf{r}_J$ corresponds to another valid configuration (because the random material is cylindrical), for which the solutions are given by

$$f_{n,N}^i(\mathbf{R}_\phi \sigma) = e^{i(N-n)\phi} f_{n,N}^i(\sigma). \quad (\text{E } 1)$$

This tells us how the rotation of a configuration modifies the coefficient $\mathfrak{F}_{n,N}$, using equation (2.16):

$$\mathfrak{F}_{n,N}(\mathbf{R}_\phi\sigma) = \sum_{i=1}^J \sum_{n'=-\infty}^{+\infty} \overline{\mathbb{V}_{n-n'}(k\mathbf{r}_i)} e^{i(N-n)\phi} f_{n',N}^i(\sigma). \quad (\text{E } 2)$$

Consequently,

$$\langle \mathfrak{F}_{n,N} \rangle = \int_{\sigma} \mathfrak{F}_{n,N}(\sigma) p(\sigma) d\sigma = \int_{\sigma} \frac{1}{2\pi} \int_0^{2\pi} \mathfrak{F}_{n,N}(\mathbf{R}_\phi\sigma) p(\sigma) d\sigma d\phi = \delta_{n-N} \int_{\sigma} \mathfrak{F}_{n,N}(\sigma) p(\sigma) d\sigma, \quad (\text{E } 3)$$

where δ_n is defined by equation (2.20). Finally, we deduce

$$\mathcal{T}_{n,N} = \delta_{n-N} \int \mathfrak{F}_{n,N}(\mathbf{r}_1, \dots, \mathbf{r}_J) p(\mathbf{r}_1, \dots, \mathbf{r}_J) d\mathbf{r}_1, \dots, d\mathbf{r}_J. \quad (\text{E } 4)$$

This analysis proves that only the diagonal terms of the effective T-matrix are non-zero and can be estimated by $\mathcal{T}_{n,n} = \langle \mathfrak{F}_{n,n} \rangle$.

References

- Gumerov NA, Duraiswami R. 2005 Computation of scattering from clusters of spheres using the fast multipole method. *J. Acoust. Soc. Am.* **117**, 1744–1761. (doi:10.1121/1.1853017)
- Koc S, Chew WC. 1998 Calculation of acoustical scattering from a cluster of scatterers. *J. Acoust. Soc. Am.* **103**, 721–734. (doi:10.1121/1.421231)
- Mishchenko MI, Travis LD, Lacis AA. 2006 *Multiple scattering of light by particles: radiative transfer and coherent backscattering*. Cambridge, UK: Cambridge University Press.
- Bennetts LG, Peter MA. 2013 Spectral analysis of wave propagation through rows of scatterers via random sampling and a coherent potential approximation. *SIAM J. Appl. Math.* **73**, 1613–1633. (doi:10.1137/120903439)
- Montiel F, Squire VA, Bennetts LG. 2015 Evolution of directional wave spectra through finite regular and randomly perturbed arrays of scatterers. *SIAM J. Appl. Math.* **75**, 630–651. (doi:10.1137/140973906)
- Montiel F, Squire VA, Bennetts LG. 2015 Reflection and transmission of ocean wave spectra by a band of randomly distributed ice floes. *Ann. Glaciol.* **56**, 315–322. (doi:10.3189/2015AoG69A556)
- Ping S. 2006 *Introduction to wave scattering, localization and mesoscopic phenomena*. Berlin, Heidelberg, Germany: Springer. (doi:10.1007/3-540-29156-3)
- Vynck K, Pierrat R, Carminati R, Froufe-Pérez LS, Scheffold F, Sapienza R, Vignolini S, Sáenz JJ. 2021 Light in correlated disordered media. *arXiv preprint arXiv:2106.13892*.
- Twersky V. 1962 On scattering of waves by random distributions. I. free-space scatterer formalism. *J. Math. Phys.* **3**, 700–715. (doi:10.1063/1.1724272)
- Twersky V. 1962 On Scattering of waves by random distributions. II. two-space scatterer formalism. *J. Math. Phys.* **3**, 724–734. (doi:10.1063/1.1724274)
- Foldy LL. 1945 The multiple scattering of waves. I. General theory of isotropic scattering by randomly distributed scatterers. *Phys. Rev.* **67**, 107–119. (doi:10.1103/PhysRev.67.107)
- Linton CM, Martin PA. 2005 Multiple scattering by random configurations of circular cylinders: second-order corrections for the effective wavenumber. *J. Acoust. Soc. Am.* **117**, 3413–3423. (doi:10.1121/1.1904270)
- Waterman PC, Truell R. 1961 Multiple scattering of waves. *J. Math. Phys.* **2**, 512–537. (doi:10.1063/1.1703737)
- Martin PA. 2003 Acoustic scattering by inhomogeneous obstacles. *SIAM J. Appl. Math.* **64**, 297–308. (doi:10.1137/S0036139902414379)
- Lax M. 1952 Multiple scattering of waves. II. The effective field in dense systems. *Phys. Rev.* **85**, 621–629. (doi:10.1103/PhysRev.85.621)
- Gower AL, Gower RM, Deakin J, Parnell WJ, David Abrahams I. 2018 Characterising particulate random media from near-surface backscattering: a machine learning approach to predict particle size and concentration. *Europhys. Lett.* **122**, 54001. (doi:10.1209/0295-5075/122/54001)

17. Karnezis A, Piva PS, Gower AL. 2024 The average transmitted wave in random particulate materials. *New J. Phys.* **26**, 063002. (doi:10.1088/1367-2630/ad49c2)
18. Chekroun M, Le Marrec L, Lombard B, Piraux J. 2012 Time-domain numerical simulations of multiple scattering to extract elastic effective wavenumbers. *Waves Random Complex Media* **22**, 398–422. (doi:10.1080/17455030.2012.704432)
19. Gower AL, Kristensson G. 2021 Effective waves for random three-dimensional particulate materials. *New J. Phys.* **23**, 063083. (doi:10.1088/1367-2630/abdfce)
20. Montiel F, Meylan MH, Hawkins SC. 2024 Scattering kernel of an array of floating ice floes: application to water wave transport in the marginal ice zone. *Proc. R. Soc. A* **480**, 2024. (doi:10.1098/rspa.2023.0633)
21. Bose SK, Mal AK. 1973 Longitudinal shear waves in a fiber-reinforced composite. *Int. J. Solids Struct.* **9**, 1075–1085. (doi:10.1016/0020-7683(73)90016-4)
22. Ni Y, Gao L, Qiu CW. 2010 Achieving invisibility of homogeneous cylindrically anisotropic cylinders. *Plasmonics* **5**, 251–258. (doi:10.1007/s11468-010-9145-8)
23. Pendry JB, Smith DR. 2004 Reversing light with negative refraction. *Phys. Today* **57**, 37–43. (doi:10.1063/1.1784272)
24. Dubois J, Aristégui C, Poncelet O, Shuvalov AL. 2011 Coherent acoustic response of a screen containing a random distribution of scatterers: comparison between different approaches. *J. Phys: Conf. Ser.* **269**, 012004. (doi:10.1088/1742-6596/269/1/012004)
25. Linton CM, Martin PA. 2005 Multiple scattering by random configurations of circular cylinders: second-order corrections for the effective wavenumber. *J. Acoust. Soc. Am.* **117**, 3413–3423. (doi:10.1121/1.1904270)
26. Rohfritsch A, Conoir JM, Marchiano R, Valier-Brasier T. 2019 Numerical simulation of two-dimensional multiple scattering of sound by a large number of circular cylinders. *J. Acoust. Soc. Am.* **145**, 3320–3329. (doi:10.1121/1.5110310)
27. Tishkovets VP, Petrova EV, Mishchenko MI. 2011 Scattering of electromagnetic waves by ensembles of particles and discrete random media. *J. Quant. Spectroscopy Radi. Transfer* **112**, 2095–2127. (doi:10.1016/j.jqsrt.2011.04.010)
28. Torrent D, Håkansson A, Cervera F, Sánchez-Dehesa J. 2006 Homogenization of two-dimensional clusters of rigid rods in air. *Phys. Rev. Lett.* **96**, 204302. (doi:10.1103/PhysRevLett.96.204302)
29. Tsang L, Kong JA, Habashy T. 1982 Multiple scattering of acoustic waves by random distribution of discrete spherical scatterers with the quasicrystalline and Percus–Yevick approximation. *J. Acoust. Soc. Am.* **71**, 552–558. (doi:10.1121/1.387524)
30. Varadan VK, Brongi VN, Varadan VV, Ishimaru A. 1983 Multiple scattering theory for waves in discrete random media and comparison with experiments. *Radio Sci.* **18**, 321–327. (doi:10.1029/RS018i003p00321)
31. Cotterill PA, Nigro D, Parnell WJ. 2022 Deeply subwavelength giant monopole elastodynamic metacluster resonators. *Proc. R. Soc. A* **478**, 20220026. (doi:10.1098/rspa.2022.0026)
32. Smith MJA, Abrahams ID. 2022 Tailored acoustic metamaterials. Part I. Thin- and thick-walled Helmholtz resonator arrays. *Proc. R. Soc. A* **478**, 20220124. (doi:10.1098/rspa.2022.0124)
33. Smith MJA, Cotterill PA, Nigro D, Parnell WJ, Abrahams ID. 2022 Asymptotics of the meta-atom: plane wave scattering by a single Helmholtz resonator. *Phil. Trans. R. Soc. A* **380**, 20210383. (doi:10.1098/rsta.2021.0383)
34. Gower AL, Smith MJA, Parnell WJ, Abrahams ID. 2018 Reflection from a multi-species material and its transmitted effective wavenumber. *Proc. R. Soc. A* **474**, 20170864. (doi:10.1098/rspa.2017.0864)
35. Martin PA. 2006 Multiple scattering. *Multiple scattering: interaction of time-harmonic waves with N obstacles*. Cambridge, UK: Cambridge University Press. (doi:10.1017/CBO9780511735110)
36. Ganesh M, Hawkins SC. 2017 Algorithm 975: Tmatrom—a t-matrix reduced order model software. *ACM Transact. Math. Software (TOMS)* **44**, 1–18.
37. Challis RE, Povey MJW, Mather ML, Holmes AK. 2005 Ultrasound techniques for characterizing colloidal dispersions. *Rep. Prog. Phys.* **68**, 1541–1637. (doi:10.1088/0034-4885/68/7/R01)

38. Kong JA, Tsang L, Ding KH, Ao CO. 2004 *Scattering of electromagnetic waves: numerical simulations*. Hoboken, NY: John Wiley & Sons.
39. Banetta L, Leone F, Anzivino C, Murillo MS, Zaccone A. 2022 Microscopic theory for the pair correlation function of liquidlike colloidal suspensions under shear flow. *Phys. Rev. E* **106**, 044610. (doi:10.1103/PhysRevE.106.044610)
40. Percus JK, Yevick GJ. 1958 Analysis of classical statistical mechanics by means of collective coordinates. *Phys. Rev.* **110**, 1–13. (doi:10.1103/PhysRev.110.1)
41. Gower AL, Parnell WJ, Abrahams ID. 2019 Multiple waves propagate in random particulate materials. *SIAM J. Appl. Math.* **79**, 2569–2592. (doi:10.1137/18M122306X)
42. Gower AL, Abrahams ID, Parnell WJ. 2019 A proof that multiple waves propagate in ensemble-averaged particulate materials. *Proc. R. Soc. A* **475**, 20190344. (doi:10.1098/rspa.2019.0344)
43. Napal K. 2024 Dataset: effective T-matrix of a cylinder filled with a random 2d particulate. *Zenodo*. See <https://doi.org/10.5281/zenodo.10519872>.
44. Napal K. 2024 Effectivetmatrix.Jl: A Julia library for computing the effective T-matrix of a random particulate sphere or cylinder. *Zenodo*. See <https://doi.org/10.5281/zenodo.10529120>.
45. Elliott SJ, Orita M, Cheer J. 2020 Active control of the sound power scattered by a locally-reacting sphere. *J. Acoust. Soc. Am.* **147**, 1851. (doi:10.1121/10.0000843)
46. Kuehn C. 2016 Moment closure—a brief review. In *Control of self-organizing Nonlinear systems, Chapter 13*, pp. 253–271. Springer International Publishing. (doi:10.1007/978-3-319-28028-8)